SANDIA REPORT

Mechanical Properties of Thermal Protection System Materials

Moo Y. Lee, John H. Hofer, David R. Bronowski and Robert D. Hardy

Approved for public release; further dissemination unlimited

Sandia National Laboratories

Mechanical Properties of Thermal Protection System Materials

Moo Y. Lee, John H. Hofer, David R. Bronowski and Robert D. Hardy

Geomechanics Department
Sandia National Laboratories
P.O. Box 5800
Albuquerque, NM 87185-0751

ABSTRACT

An experimental study was conducted to measure the mechanical properties of the Thermal Protection System (TPS) materials used for the Space Shuttle. Three types of TPS materials (LI-900, LI-2200, and FRCI-12) were tested in "in-plane" and "out-of-plane" orientations. Four types of quasi-static mechanical tests (uniaxial tension, uniaxial compression, uniaxial strain, and shear) were performed under low (10^{-4} to 10^{-3}/s) and intermediate (1 to 10/s) strain rate conditions. In addition, split Hopkinson pressure bar tests were conducted to obtain the strength of the materials under a relatively higher strain rate (~10^2 to 10^3/s) condition. In general, TPS materials have higher strength and higher Young's modulus when tested in "in-plane" than in "through-the-thickness" orientation under compressive (unconfined and confined) and tensile stress conditions. In both stress conditions, the strength of the material increases as the strain rate increases. The rate of increase in LI-900 is relatively small compared to those for the other two TPS materials tested in this study. But, the Young's modulus appears to be insensitive to the different strain rates applied. The FRCI-12 material, designed to replace the heavier LI-2200, showed higher strengths under tensile and shear stress conditions. But, under a compressive stress condition, LI-2200 showed higher strength than FRCI-12. As far as the modulus is concerned, LI-2200 has higher Young's modulus both in compression and in tension. The shear modulus of FRCI-12 and LI-2200 fell in the same range.

ACKNOWLEDGEMENTS

Table of Contents

Figures

Tables

1. Introduction

NASA is currently studying the performance of the Thermal Protection System (TPS) materials in support of detailed TPS model development for the Orbiter Return to Flight Effort. This report describes an experimental study that has been completed to develop constitutive relationships for LI-900, LI-2200, and FRCI-12 tiles under different mechanical loading conditions.

The High-temperature Reusable Surface Insulation (or HRSI) tiles consist of a low-density, high-purity silica 99.8 % amorphous fiber insulation coated with a mixture of powdered tetrasilicide and borosilicate glass with a liquid carrier. The operating temperature of HRSI ranges from 1,200 to 2,300°F. Depending on the heat loading encountered during the re-entry of the orbiter into the atmosphere, the thickness of the tiles varies from one to five inches. There are also two different densities of HRSI tiles along with different thicknesses. The high-density LI-2200 (22-pcf) tiles are used in the areas such as the nose, main landing gears, external tank, and others susceptible to high heat loading. The low-density LI-900 (9-pcf) tiles are used in the areas subjected to low heat loading. The FRCI-12 tiles are made from the mixture of AB312 (alumina-borosilicate fiber) and the pure silica tile slurry. The FRCI-12 tiles are used to replace the LI-2200 tiles. The FRCI-12 tiles are designed to provide improved strength and resistance to the coating's sensitivity cracking with a relatively lower density of 12-pcf compared to LI-2200 (NASA, 1988).

The objective of this laboratory testing program was to obtain mechanical properties of the HRSI tiles under quasi-static loading conditions so that the impact modeling effort could develop and test its models and codes using realistic parameters obtained from different tile materials under various loading conditions. The experimental programs were designed to provide the fundamental parameters necessary for the simulations and analyses of the impact of foreign objects such as foam into the HRSI tiles as well as to give insight into the failure phenomena of the TPS materials.

The three types of TPS materials were tested in "In-Plane (IP)" and "Through-The-Thickness (TTT)" orientations. Four types of quasi-static mechanical tests (uniaxial tension, uniaxial compression, uniaxial strain, and shear) were performed under low (10^{-4} to 10^{-3}/s) and intermediate (1 to 10 /s) strain rate conditions. In addition, the split Hopkinson pressure bar test were conducted to obtain the strength of the materials under a dynamic ($\sim 10^{2}$ to 10^{3}/s) condition. For each TPS material, the mechanical properties of the material are obtained and the results are presented as functions of loading type, loading orientation, and applied strain rate.

2. Uniaxial Tension Test (Quasi-static and Intermediate Strain Rates)

To measure the uniaxial tensile strength of the TPS materials, specimens of LI-900, FRCI-12 and LI-2200 were provided by Boeing Huntington Beach M&PE (Materials and Process Engineering). All tensile test coupons were fabricated at Boeing Huntington Beach. Tensile Specimens have nominal dimensions of $1.0" \times 1.0" \times 2.2"$ ($\pm 0.005"$) in the shape of rectangular prism. The specimens were weighed, then bonded to aluminum end-caps using Devcon® 5 Minute Epoxy (Slenk, 2004). Figure 1 shows the specimen configuration for the tensile test. After tensile specimens have been fabricated they were inspected by the Responsible Testing Engineer (RTE) from Boeing and then sent to Sandia National Laboratories for testing.

The prepared specimens with end-caps were mounted in pivoting holding fixtures (Figure 2) in a 2.2 kip testing machine. After the specimen was secured and aligned in the pivoting fixtures, the specimen was pulled at the targeted stroke rates of 0.003"/s and 10"/s corresponding to average axial strain rates of -0.0008/s and -2.3/s. The resulting strain rates varied for different TSP materials and orientations of the specimen with respect to loading direction (Table A1 through A3 in Appendix A). Two Linear Variable Displacement Transformers (LVDTs) were mounted on the specimen in parallel with the loading axis (Figure 3). The LVDTs were placed on a "V-groove" of the rectangular base plate. The groove was machined to be parallel with the edges of the plate that was aligned with the long axis of the specimen. The width of the plate was designed to have the same width of the specimen (1.0"). This allows the LVDT aligned with the long axis of the specimen by just aligning the edge of the base plate to the specimen (Figure 3). The LVDTs are fixed to the base plate using rubber bands such that they do not induce stress concentrations in the tensile specimen.

The tensile strength of the material was calculated from the following equation:

$$-T_{ut} = P_{ut}/ (w^2)$$

where T_{ut} is the uniaxial tensile strength in psi; P_{ut} is the peak load in lbs; w is the width of the specimen in inches. The sign convention used in this report is positive for compressive stress and strain and negative for tensile stress and strain.

The rectangular prism-shaped specimen is usually suitable for compression testing. If this configuration is implemented in uniaxial tension testing, however, the specimen usually fails near the end of the specimen where the end-cap is bonded. Due to mismatches in elastic properties between the specimen and the end-cap, stresses can be concentrated near the ends of the specimen. Uniform cross-sectional area (1 inch^2) of the specimen perpendicular to the loading direction may not allow the specimen to fail in tension away from the ends of the specimen. In this study, the rectangular prism specimens were used for uniaxial tension tests regardless of the limitations so the tensile test results could be compared to the archived historical data set which was obtained using the same configuration (Slenk, 2005). It is recommended to use shaped specimens (e.g. dubmbell shape, see Figure 6) for future tension testing to induce the failure surface (Figure 4) away from the ends of the specimen.

Figure 5 shows a uniaxial tension test record for a FRCI-12 sample tested at a quasi-static strain rate of -0.0007/s. The test record consists of axial stress vs. axial strain plots (LVDT-1, LVDT-2, and the average of those two shown as ε_a-avg). The tensile strength of the material is obtained from the peak stress and Young's modulus is calculated from the slope of the ascending portion of the stress-strain curve. Table 1 shows the test matrix for the uniaxial tension tests. Tables A1 through A3, in Appendix A, summarize the results from the uniaxial tension tests conducted for three TPS materials in two orthogonal orientations at two different strain rates.
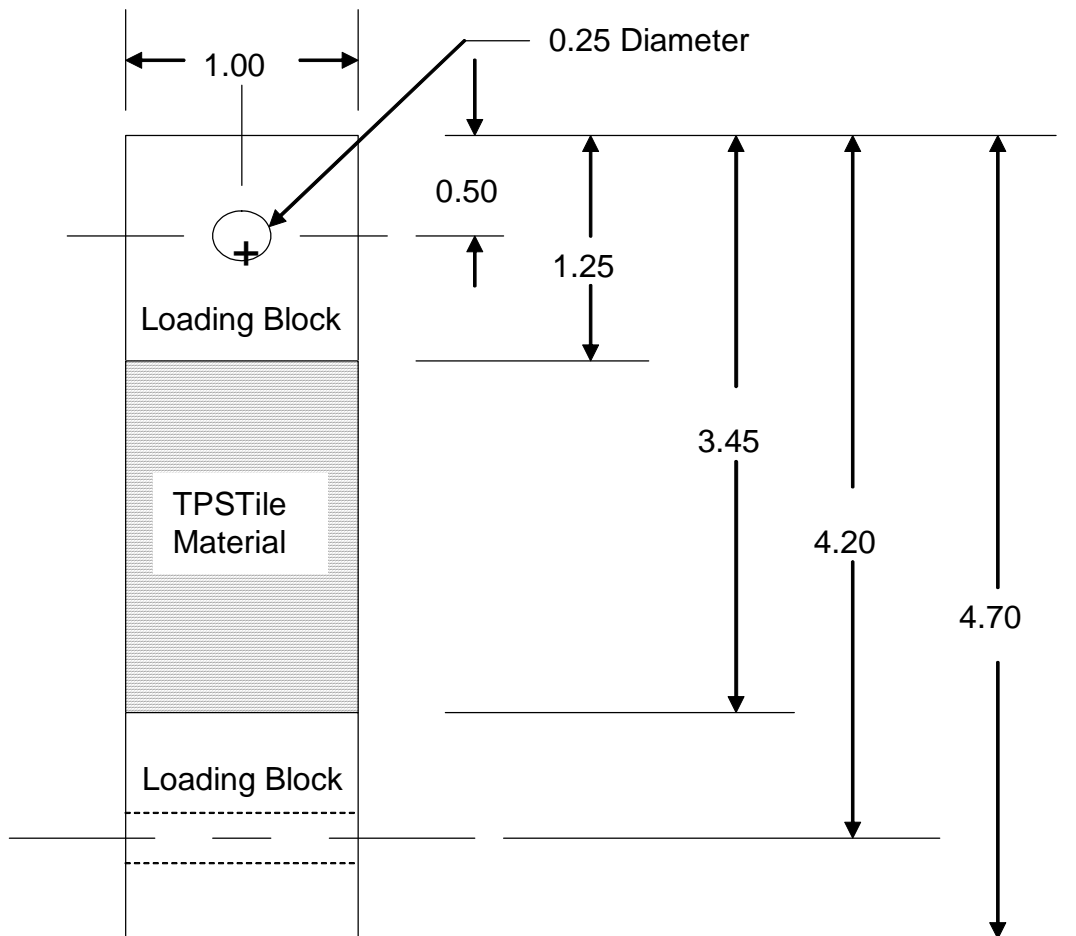
Figure 1. Schematic of the tension test specimen provided by Boeing (All dimensions are in inches.)
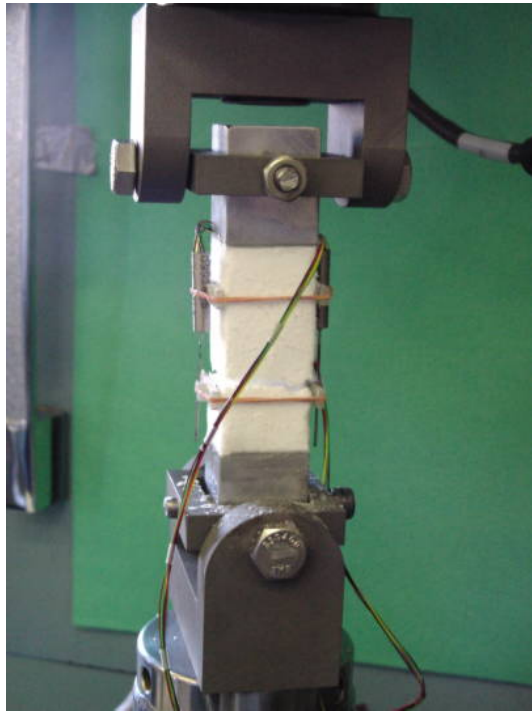
Figure 2. Typical uniaxial tension test set-up with pivoting universal joints connected to both ends of the end-caps.
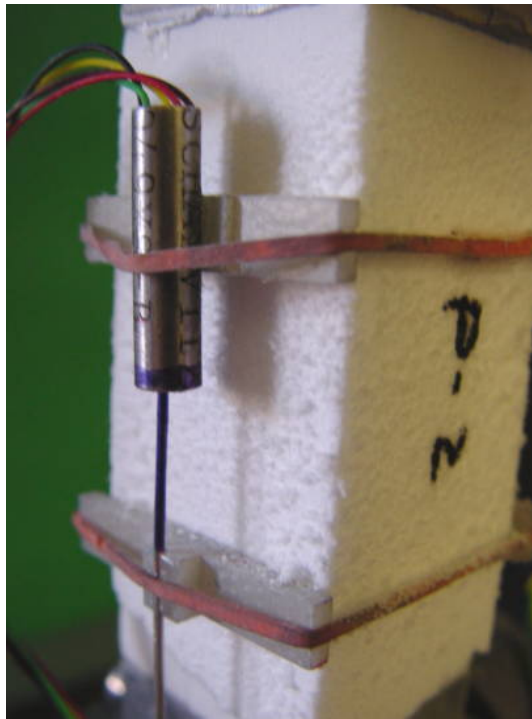
Figure 3. An LVDT directly mounted on the side of the specimen to measure the axial displacement of the specimen. Two LVDTs (an LVDT is on opposite side of the specimen) are aligned in parallel with the loading axis using the "V-groove" of the base plates.
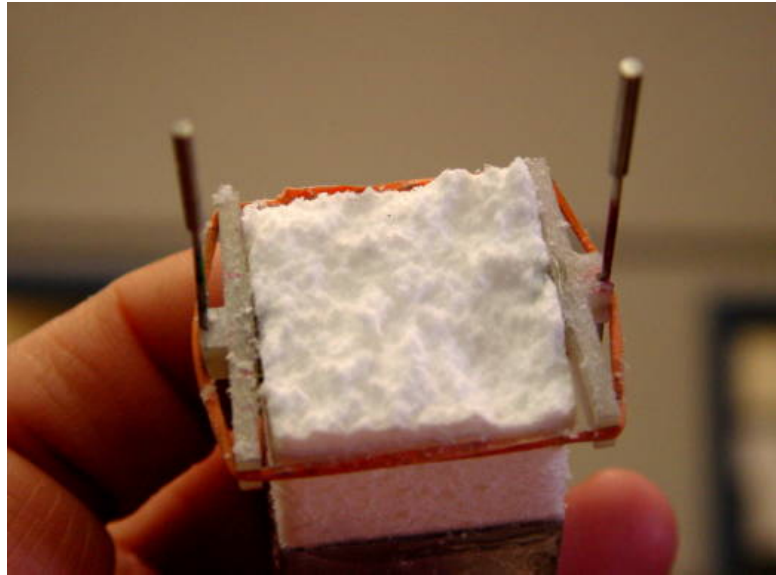
Figure 4. A tensile failure surface of the specimen perpendicular to the loading axis. Also shown are two cores of the LVDTs mounted on the specimen along the loading axis.
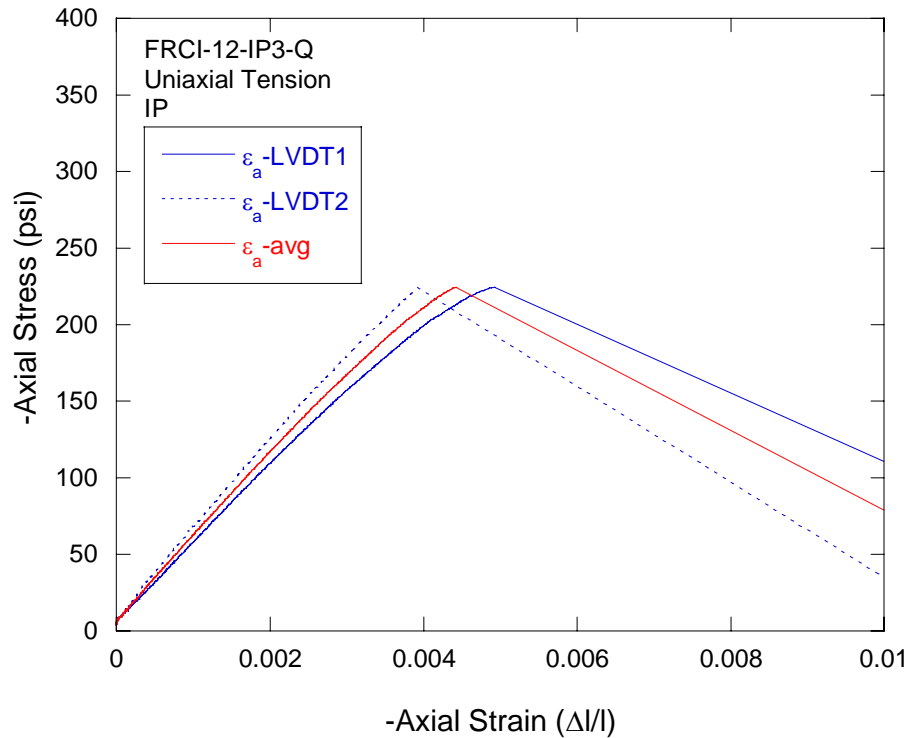
Figure 5. Stress-strain plots obtained during the uniaxial tension test for the FRCI-12-IP3-Q specimen. The axial stress is plotted against the axial (ε_a) strains obtained from LVDT-1, LVDT-2, and the average of those two results.

Table 1. Uniaxial tension test matrix for the Thermal Protection System (TPS) Materials.

Test ID	Material	Orientation*	Stroke Rate** (inch/s)
LI-900-IP1-Q	LI-900	IP	0.003
LI-900-IP2-Q	LI-900	IP	0.003
LI-900-IP3-Q	LI-900	IP	0.003
LI-900-IP4-Q	LI-900	IP	0.003
LI-900-IP5-Q	LI-900	IP	0.003
LI-900-IP7-10	LI-900	IP	10
LI-900-IP8-10	LI-900	IP	10
LI-900-IP9-10	LI-900	IP	10
LI-900-IP10-10	LI-900	IP	10
LI-900-IP12-10	LI-900	IP	10
LI-900-T1-Q	LI-900	TTT	0.003
LI-900-T2-Q	LI-900	TTT	0.003
LI-900-T3-Q	LI-900	TTT	0.003
LI-900-T4-Q	LI-900	TTT	0.003
LI-900-T5-Q	LI-900	TTT	0.003
LI-900-T7-10	LI-900	TTT	10
LI-900-T8-10	LI-900	TTT	10
LI-900-T9-10	LI-900	TTT	10
LI-900-T10-10	LI-900	TTT	10
LI-900-T11-10	LI-900	TTT	10
LI-2200-IP1-Q	LI-2200	IP	0.003
LI-2200-IP3-Q	LI-2200	IP	0.003
LI-2200-IP4-Q	LI-2200	IP	0.003
LI-2200-IP11-Q	LI-2200	IP	0.003
LI-2200-IP12-Q	LI-2200	IP	0.003
LI-2200-IP6-10	LI-2200	IP	10
LI-2200-IP7-10	LI-2200	IP	10
LI-2200-IP8-10	LI-2200	IP	10
LI-2200-IP9-10	LI-2200	IP	10
LI-2200-IP10-10	LI-2200	IP	10
LI-2200-T1-Q	LI-2200	TTT	0.003
LI-2200-T2-Q	LI-2200	TTT	0.003
LI-2200-T3-Q	LI-2200	TTT	0.003
LI-2200-T4-Q	LI-2200	TTT	0.003
LI-2200-T5-Q	LI-2200	TTT	0.003
LI-2200-T7-10	LI-2200	TTT	10
LI-2200-T8-10	LI-2200	TTT	10
LI-2200-T9-10	LI-2200	TTT	10
LI-2200-T10-10	LI-2200	TTT	10
LI-2200-T13-10	LI-2200	TTT	10
FRCI-12-IP2-Q	FRCI-12	IP	0.003
FRCI-12-IP3-Q	FRCI-12	IP	0.003

Table 1. Uniaxial tension test matrix for the Thermal Protection System (TPS) Materials (continued).

Test ID	Material	Orientation*	Stroke Rate** (inch/s)
FRCI-12-IP4-Q	FRCI-12	IP	0.003
FRCI-12-IP5-Q	FRCI-12	IP	0.003
FRCI-12-IP11-Q	FRCI-12	IP	0.003
FRCI-12-IP6-10	FRCI-12	IP	10
FRCI-12-IP7-10	FRCI-12	IP	10
FRCI-12-IP8-10	FRCI-12	IP	10
FRCI-12-IP9-10	FRCI-12	IP	10
FRCI-12-IP10-10	FRCI-12	IP	10
FRCI-12-T1-Q	FRCI-12	TTT	0.003
FRCI-12-T2-Q	FRCI-12	TTT	0.003
FRCI-12-T3-Q	FRCI-12	TTT	0.003
FRCI-12-T4-Q	FRCI-12	TTT	0.003
FRCI-12-T5-Q	FRCI-12	TTT	0.003
FRCI-12-T6-10	FRCI-12	TTT	10
FRCI-12-T7-10	FRCI-12	TTT	10
FRCI-12-T8-10	FRCI-12	TTT	10
FRCI-12-T9-10	FRCI-12	TTT	10
FRCI-12-T10-10	FRCI-12	TTT	10

* IP- "In-Plane"; TTT-"Through-The-Thickness"
** The resulting axial strain rates for each test can be found in Tables A1 through A3 in Appendix A.

3. Uniaxial Compression Test (Quasi-static and Intermediate Strain Rates)

All compression test coupons of LI-900, FRCI-12 and LI-2200 were fabricated at Boeing Huntington Beach. Compression specimens were fabricated to have a 3.5" long dumbbell shape with a square cross section. Figure 6 shows the schematic of the compression test specimen (Slenk, 2004). After compression specimens have been fabricated, labeled and weighed, they were inspected by the RTE and then sent to Sandia National Laboratories for testing.

Specimens were mounted between two parallel loading platens in a 2.2 kip loading machine and tested at strain rates of ~0.0009/s and ~3.0/s (see Tables A1 through A3 in Appendix A) resulting from the targeted stroke rates of 0.003"/s and 10"/s. Boeing M&PE advised on mounting two LVDTs (Figure 7) such that they do not induce stress concentrations in the compression specimen. Figure 8 shows two LVDTs mounted on the specimen with a gage length of 1". In order to avoid the end effect between the specimen and the end-caps, dumbbell-shaped specimens were used for the compression test. The shaped specimen distributes the axial stress uniformly across the gaged section of the specimen. Photographs of test set-up were taken. Stress and strain were recorded during each test, and the strength and the Young's modulus of the TPS materials were calculated from the recorded data.

Figure 9 shows a uniaxial compression test record for an LI-2200 specimen tested at a quasi-static strain rate of 0.0008/s. The test record consists of the axial stress vs. axial strains (LVDT-1, LVDT-2, and the average of those two as ε_a-avg). The specimens were loaded until the peak load was reached. The unconfined uniaxial compressive strength of the TPS material was calculated from the following equation:

$$C_o = P_{uc}/w^2$$

where C_o is the unconfined uniaxial compressive strength of the tile material in psi; P_{uc} is the peak compressive load in lbs; and w is the width of the specimen in inches at the midheight of the specimen.

The proportional constant between stress and strain in the elastic portion of compression tests defines the Young's modulus, E. The Young's modulus was determined using least square fits of a straight line (or linear regression analysis) to the ascending linear portion of the stress-strain curve. Table 2 shows the test matrix for the uniaxial compression tests. A summary of the uniaxial compressive test results is shown in Appendix A, Tables A1 through A3.
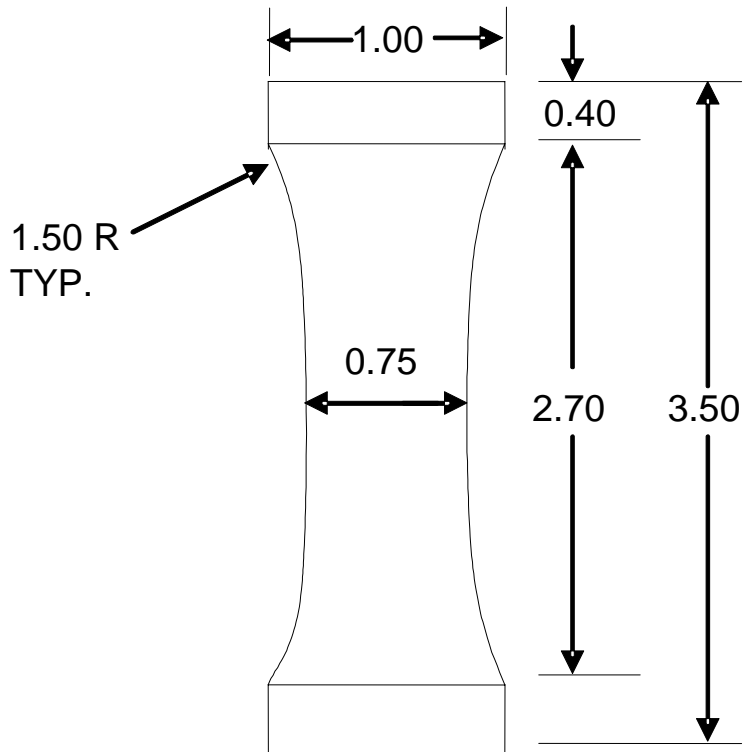
Figure 6. Schematic of compression test specimen (All dimensions are in inches.)
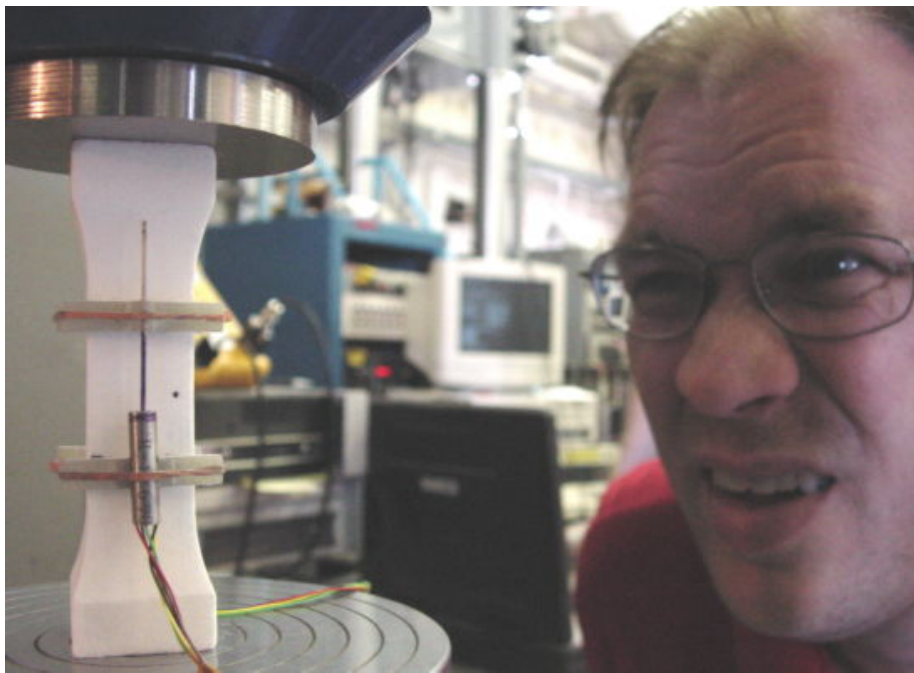
Figure 7. RTE (Responsible Testing Engineer from Boeing) inspects a dumbbell-shaped specimen used for compression tests to obtain compressive strength and modulus of the Thermal Protection System (TPS) materials.
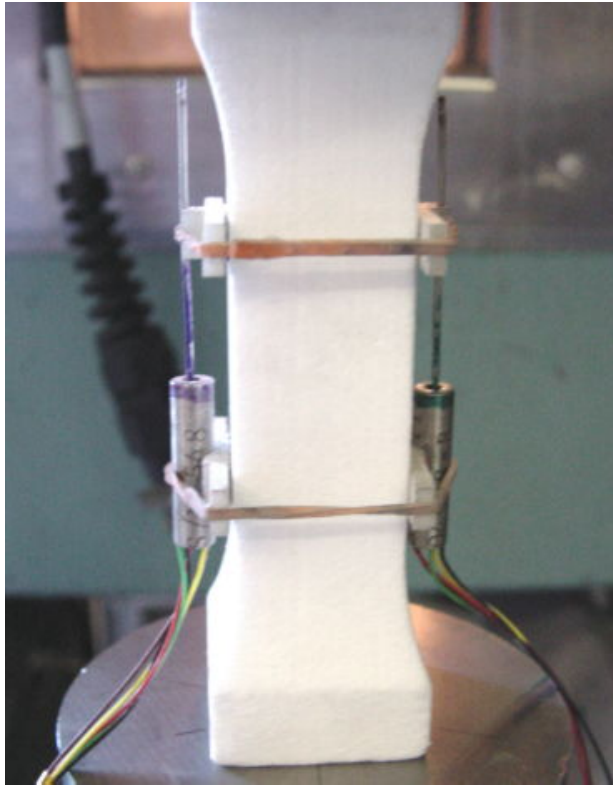
Figure 8. Two LVDTs mounted on the specimen during uniaxial compression testing.
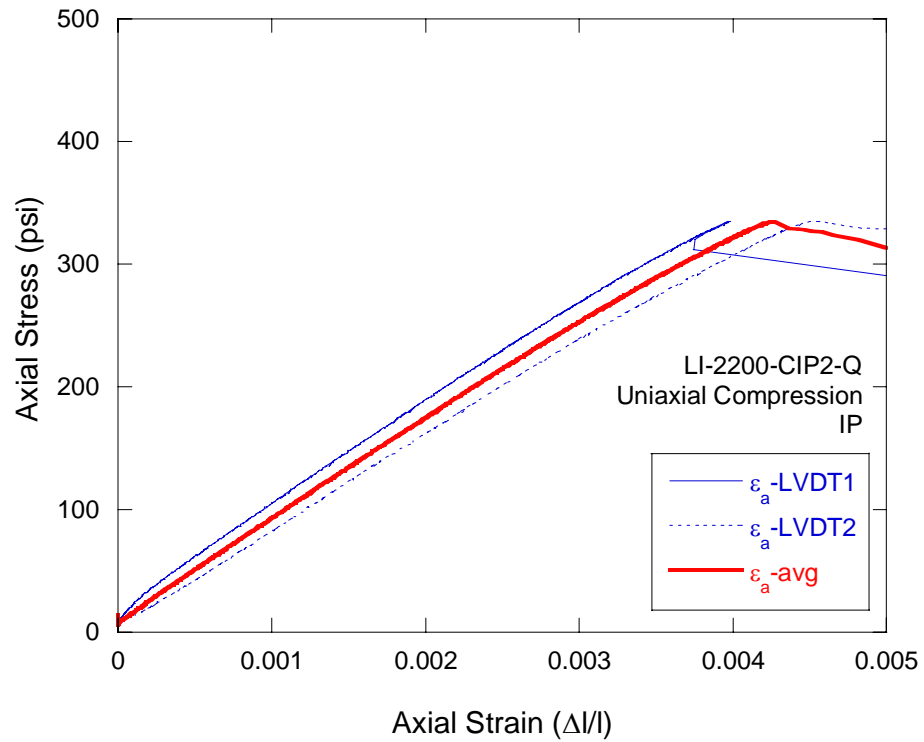
Figure 9. Stress-strain plots obtained during the unconfined uniaxial compression test for the LI-2200-CIP2-Q specimen. The axial stress (σ_a) is plotted against axial (ε_a) strains.

Table 2. Uniaxial compression test matrix for the Thermal Protection System (TPS) Materials.

Test ID	Material	Orientation*	Stroke Rate** (inch/s)
LI-900-CIP1-Q	LI-900	IP	0.003
LI-900-CIP2-Q	LI-900	IP	0.003
LI-900-CIP3-Q	LI-900	IP	0.003
LI-900-CIP4-Q	LI-900	IP	0.003
LI-900-CIP5-Q	LI-900	IP	0.003
LI-900-CIP6-10	LI-900	IP	10
LI-900-CIP7-10	LI-900	IP	10
LI-900-CIP8-10	LI-900	IP	10
LI-900-CIP9-10	LI-900	IP	10
LI-900-CIP10-10	LI-900	IP	10
LI-900-CT1R-Q	LI-900	TTT	0.003
LI-900-CT2-Q	LI-900	TTT	0.003
LI-900-CT3-Q	LI-900	TTT	0.003
LI-900-CT4-Q	LI-900	TTT	0.003
LI-900-CT5-Q	LI-900	TTT	0.003
LI-900-CT6-10	LI-900	TTT	10
LI-900-CT7-10	LI-900	TTT	10
LI-900-CT8-10	LI-900	TTT	10
LI-900-CT9-10	LI-900	TTT	10
LI-900-CT10-10	LI-900	TTT	10
LI-2200-CIP1-Q	LI-2200	IP	0.003
LI-2200-CIP2-Q	LI-2200	IP	0.003
LI-2200-CIP3-Q	LI-2200	IP	0.003
LI-2200-CIP4-Q	LI-2200	IP	0.003
LI-2200-CIP5-Q	LI-2200	IP	0.003
LI-2200-CIP6-10	LI-2200	IP	10
LI-2200-CIP7-10	LI-2200	IP	10
LI-2200-CIP8-10	LI-2200	IP	10
LI-2200-CIP9-10	LI-2200	IP	10
LI-2200-CIP10-10	LI-2200	IP	10
LI-2200-CT1-Q	LI-2200	TTT	0.003
LI-2200-CT2-Q	LI-2200	TTT	0.003
LI-2200-CT3-Q	LI-2200	TTT	0.003
LI-2200-CT4-Q	LI-2200	TTT	0.003
LI-2200-CT5-Q	LI-2200	TTT	0.003
LI-2200-CT6-10	LI-2200	TTT	10
LI-2200-CT7-10	LI-2200	TTT	10
LI-2200-CT8-10	LI-2200	TTT	10
LI-2200-CT9-10	LI-2200	TTT	10
LI-2200-CT10-10	LI-2200	TTT	10
FRCI-12-CIP1-Q	FRCI-12	IP	0.003
FRCI-12-CIP2-Q	FRCI-12	IP	0.003

Table 2. Uniaxial compression test matrix for the Thermal Protection System (TPS) Materials (continued).

Test ID	Material	Orientation	Stroke Rate (inch/s)
FRCI-12-CIP3-Q	FRCI-12	IP	0.003
FRCI-12-CIP4-Q	FRCI-12	IP	0.003
FRCI-12-CIP5-Q	FRCI-12	IP	0.003
FRCI-12-CIP6-10	FRCI-12	IP	10
FRCI-12-CIP9-10	FRCI-12	IP	10
FRCI-12-CIP10-10	FRCI-12	IP	10
FRCI-12-CIP13-10	FRCI-12	IP	10
FRCI-12-CT1-Q	FRCI-12	TTT	0.003
FRCI-12-CT2-Q	FRCI-12	TTT	0.003
FRCI-12-CT3-Q	FRCI-12	TTT	0.003
FRCI-12-CT4-Q	FRCI-12	TTT	0.003
FRCI-12-CT5-Q	FRCI-12	TTT	0.003
FRCI-12-CT6-10	FRCI-12	TTT	10
FRCI-12-CT7-10	FRCI-12	TTT	10
FRCI-12-CT8-10	FRCI-12	TTT	10
FRCI-12-CT9-10	FRCI-12	TTT	10
FRCI-12-CT10-10	FRCI-12	TTT	10

* IP- "In-Plane"; TTT-"Through-The-Thickness"

** The resulting axial strain rates for each test can be found in Tables A1 through A3 in Appendix A.

4. Shear Test (Quasi-static and Intermediate Strain Rates)

Boeing Huntington Beach M&PE provided the shear testing specimens of LI-900, FRCI-12 and LI-2200. Shear specimens were cut into 6.0" × 2.0" × 0.5" (± 0.005") rectangular blocks, labeled, weighed and then bonded to aluminum shear blocks using Devcon® 5 Minute Epoxy. Figure 10 shows the schematic of the shear test specimen. After shear specimens have been fabricated, they were inspected by the RTE from Boeing and then sent to Sandia National Laboratories for testing. All shear test coupons were fabricated at Boeing Huntington Beach except for the five LI-900 specimens listed in Appendix B, Table B1. These Sandia prepared specimens replaced the defective LI-900 specimens that had been delaminated from the shear block during testing.

Table 3 summarizes the shear test-matrix conducted for the TPS materials in "strong-plane" (SP) and "weak-plane" (WP) orientations at quasi-static (0.003 inch/s) and intermediate (10 inch/s) stroke rates. The SP specimens have the shear failure plane perpendicular to the plane formed by the "in-plane" orientations (Figure 11). In contrast, the WP specimens have the shear failure plane aligned in parallel with the weakness plane formed by the "in-plane" orientations (Figure 11). Two LVDTs were calibrated prior to testing and used as displacement measurement gages. As shown in Figure 12, specimens were mounted in pivoting holding fixtures provided by the Boeing M&PE. The prepared specimen was tested in a 22 kip loading machine following the test-matrix shown in Table 3. As shown in Figures 13 and 14, the LVDTs were mounted to measure the relative displacement of the aluminum shear blocks during testing. Figure 14 also shows a photograph of the failed surfaces exposed after the test. The failure surfaces always show the gouges of the TPS material from shearing.

The shear stress is calculated as:

$$\sigma_{xy} = \frac{P_s}{wL}$$

where σ_{xy} is the shear stress applied to the tile material in psi; P_s is the shear load in lbs; and w and L are the width and the length of the specimen in inches, respectively (wL≡2×6=12 inch^2 in this TPS materials testing).

The shear strain is calculated as:

$$\varepsilon_{xy} = \frac{\gamma_{xy}}{2}$$

where ε_{xy} is the shear strain, γ_{xy} is the engineering (or total) measured as the relative displacement of the block along the shear load divided by the thickness of the specimen. The shear stress vs. engineering shear strain plot was recorded during testing (Figure 15). The ultimate shear stress at failure of the specimen was obtained as the peak stress and the shear modulus, G, was calculated as follows:

$$G = \frac{\sigma_{xy}}{\gamma_{xy}}$$

The shear modulus is obtained from the slope of the ascending linear portion of the shear stress vs. engineering shear strain plot. The results are summarized in Appendix B, Table B1 through B3.
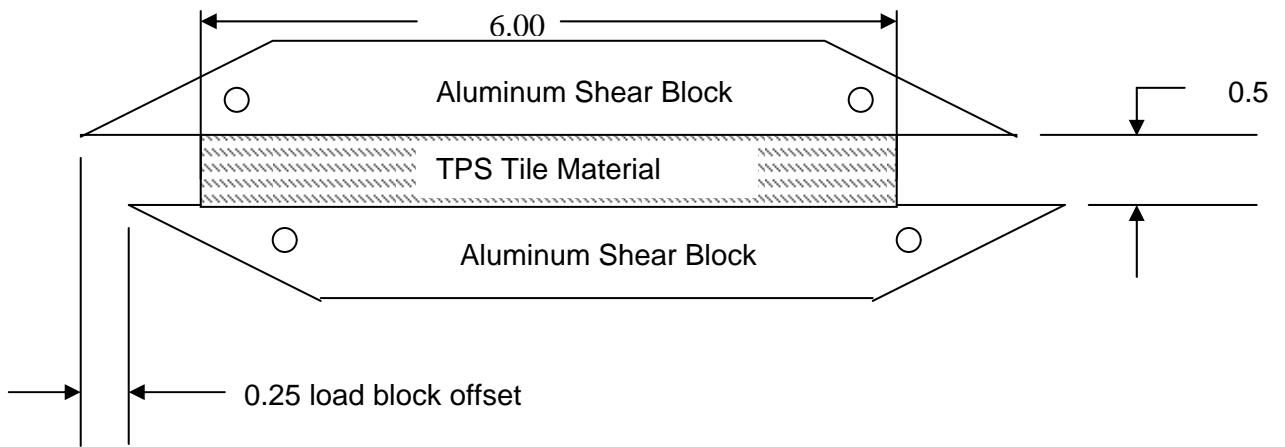
Figure 10. Schematic of the shear test specimen (All dimensions are in inches.)
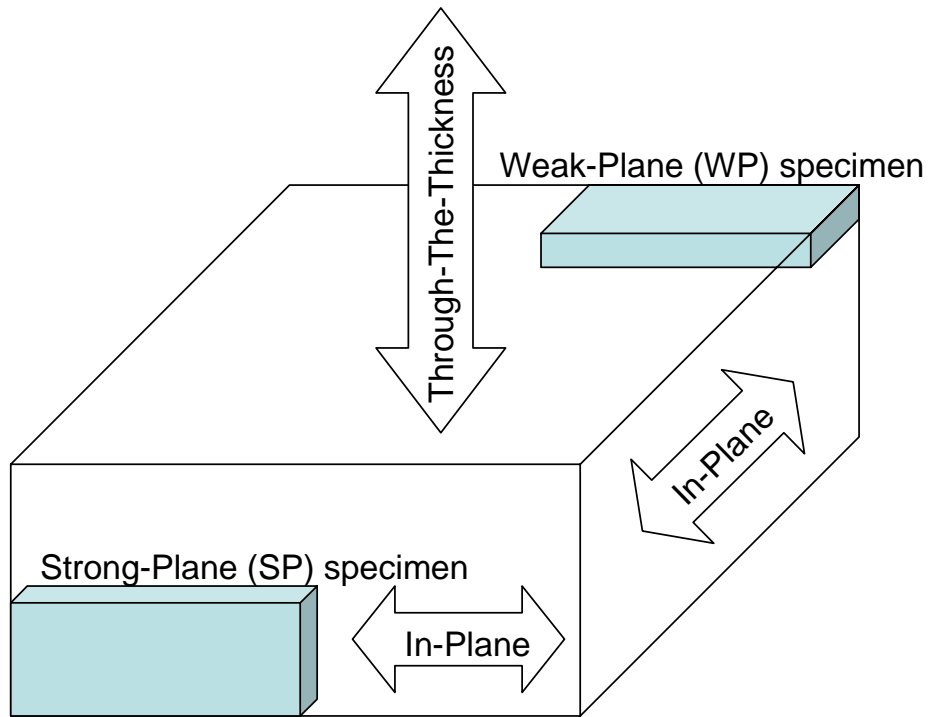
Figure 11. Orientations of "weak-plane" and "strong-plane" with respect to "in-plane" and "through-the-thickness".
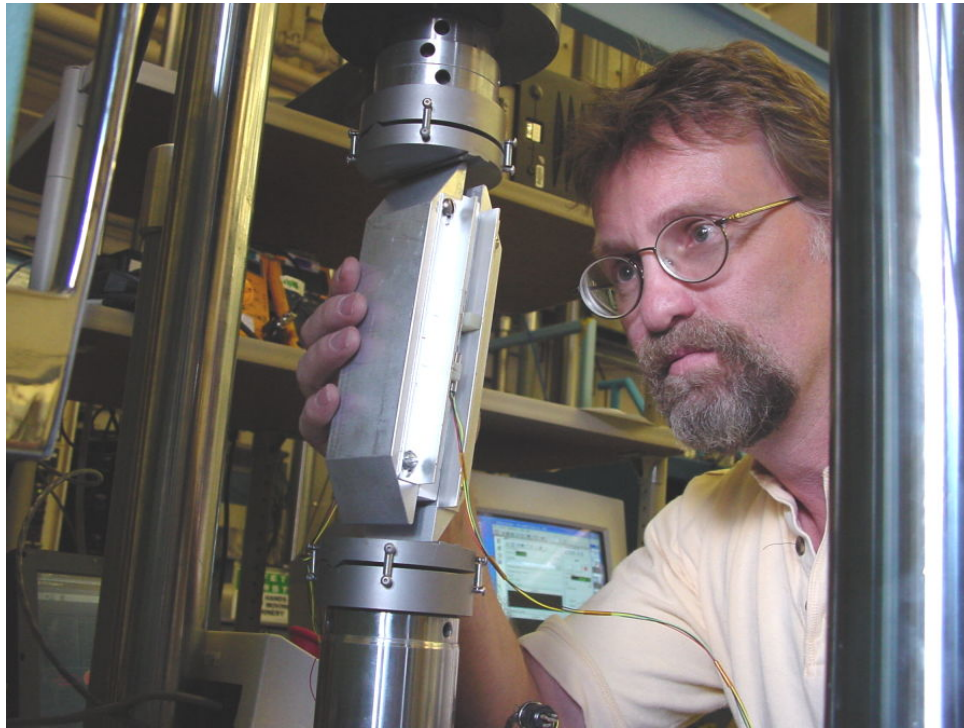
Figure 12. Typical shear test set-up with two pivoting shear fixtures and two LVDTs measuring relative displacement of shear blocks along the shearing direction.
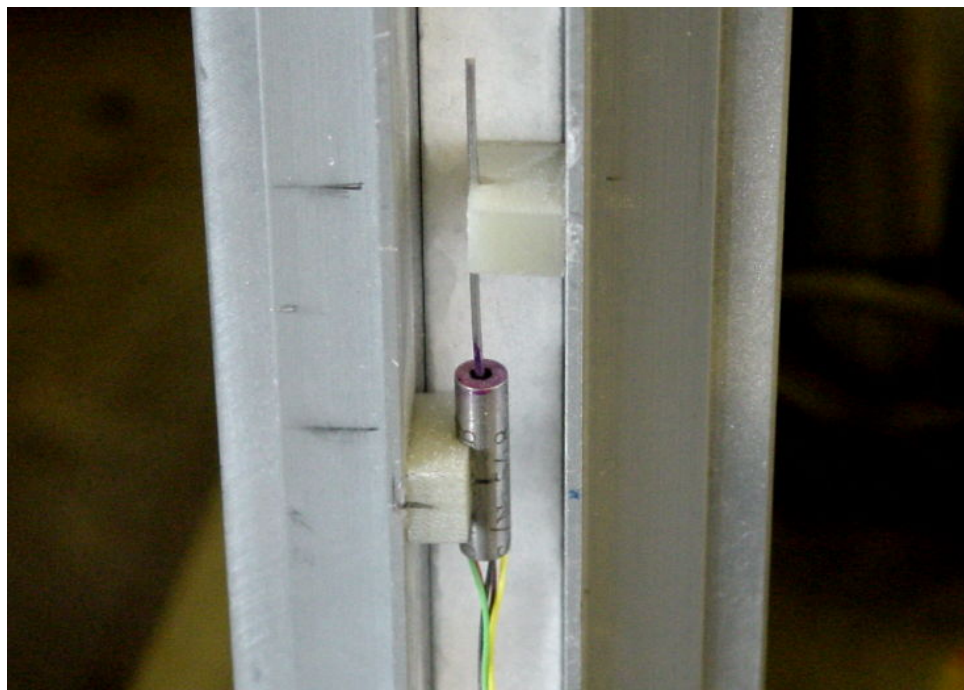
Figure 13. An LVDT mounted on the aluminum blocks to measure the relative shear displacement of the specimen.
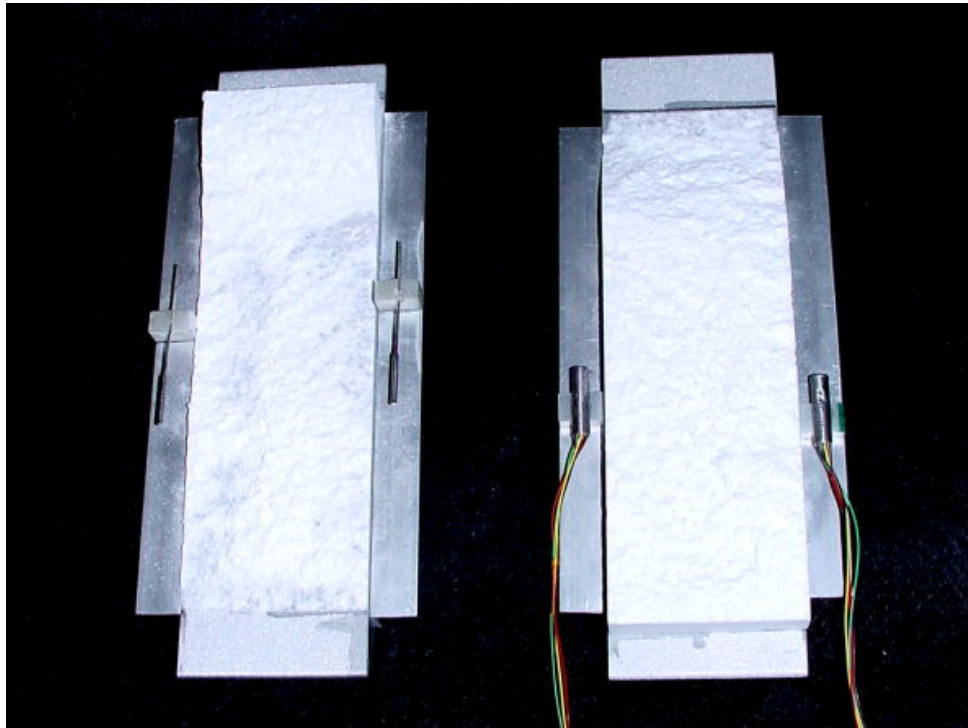
Figure 14. Shear failure surfaces of the specimen after the test. Also shown are two LVDTs mounted on the aluminum blocks.
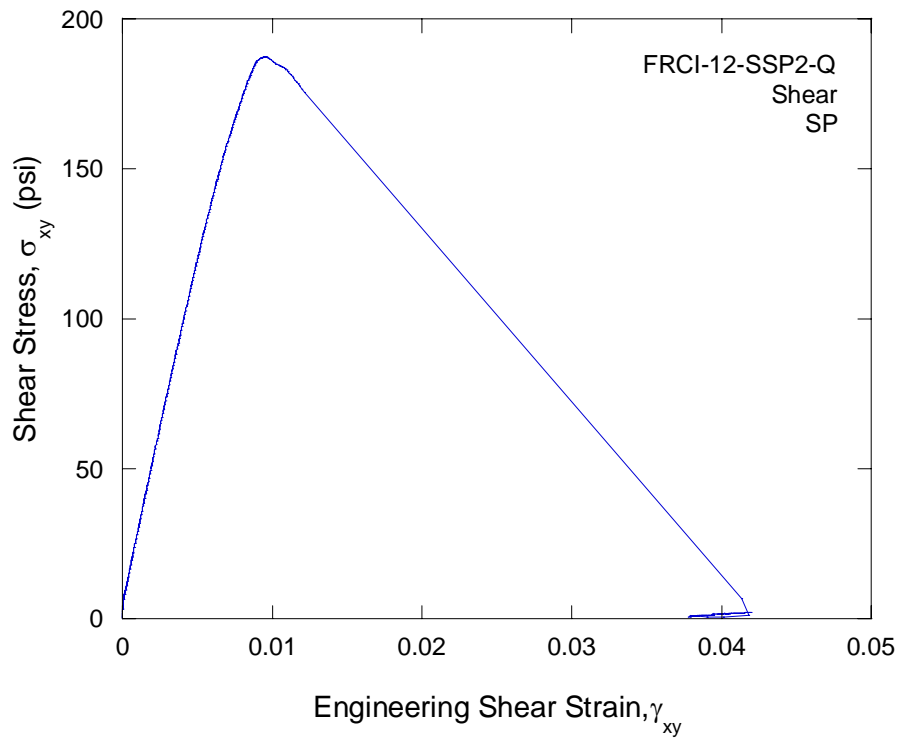
Figure 15. The shear stress versus shear strain plot obtained in shear testing of a FRCI-12 material loaded in the "Strong-Plane" (SP) orientation.

Table 3. Shear test matrix for the Thermal Protection System (TPS) Materials.

Test ID	Material	Orientation*	Stroke Rate** (inch/s)
LI-900-SWP1-Q	LI-900	WP	0.003
LI-900-SWP2-Q	LI-900	WP	0.003
LI-900-SWP3-Q	LI-900	WP	0.003
LI-900-SWP5-Q	LI-900	WP	0.003
LI-900-SWP6-Q	LI-900	WP	0.003
LI-900-SWP7-10	LI-900	WP	10
LI-900-SWP8-10	LI-900	WP	10
LI-900-SWP9-10	LI-900	WP	10
LI-900-SWP10-10	LI-900	WP	10
LI-900-SWP11-10	LI-900	WP	10
LI-900-SSP1-Q	LI-900	SP	0.003
LI-900-SSP2-Q	LI-900	SP	0.003
LI-900-SSP3-Q***	LI-900	SP	0.003
LI-900-SSP4-Q	LI-900	SP	0.003
LI-900-SSP5-Q	LI-900	SP	0.003
LI-900-SSP105-Q	LI-900	SP	0.003
LI-900-SSP6-10***	LI-900	SP	10
LI-900-SSP7-10	LI-900	SP	10
LI-900-SSP8-10***	LI-900	SP	10
LI-900-SSP9-10***	LI-900	SP	10
LI-900-SSP10-10***	LI-900	SP	10
LI-900-SSP101-10	LI-900	SP	10
LI-900-SSP102-10	LI-900	SP	10
LI-900-SSP103-10	LI-900	SP	10
LI-900-SSP104-10	LI-900	SP	10
LI-2200-SWP1-Q	LI-2200	WP	0.003
LI-2200-SWP2-Q	LI-2200	WP	0.003
LI-2200-SWP4-Q	LI-2200	WP	0.003
LI-2200-SWP5-Q	LI-2200	WP	0.003
LI-2200-SWP11-Q	LI-2200	WP	0.003
LI-2200-SWP7-10	LI-2200	WP	10
LI-2200-SWP8-10	LI-2200	WP	10
LI-2200-SWP9-10	LI-2200	WP	10
LI-2200-SWP10-10	LI-2200	WP	10
LI-2200-SWP12-10	LI-2200	WP	10
LI-2200-SSP1-Q	LI-2200	SP	0.003
LI-2200-SSP2-Q	LI-2200	SP	0.003
LI-2200-SSP3-Q	LI-2200	SP	0.003
LI-2200-SSP4-Q	LI-2200	SP	0.003
LI-2200-SSP5-Q	LI-2200	SP	0.003
LI-2200-SSP6-10	LI-2200	SP	10
LI-2200-SSP7-10***	LI-2200	SP	10

Table 3. Shear test matrix for the Thermal Protection System (TPS) Materials (continued).

Test ID	Material	Orientation	Stroke Rate** (inch/s)
LI-2200-SSP8-10***	LI-2200	SP	10
LI-2200-SSP9-10	LI-2200	SP	10
LI-2200-SSP10-10***	LI-2200	SP	10
FRCI-12-SWP1-Q	FRCI-12	WP	0.003
FRCI-12-SWP2-Q	FRCI-12	WP	0.003
FRCI-12-SWP3-Q	FRCI-12	WP	0.003
FRCI-12-SWP4-Q	FRCI-12	WP	0.003
FRCI-12-SWP5-Q	FRCI-12	WP	0.003
FRCI-12-SWP12-10	FRCI-12	WP	10
FRCI-12-SWP13-10	FRCI-12	WP	10
FRCI-12-SSP2-Q	FRCI-12	SP	0.003
FRCI-12-SSP3-Q	FRCI-12	SP	0.003
FRCI-12-SSP4-Q	FRCI-12	SP	0.003
FRCI-12-SSP5-Q	FRCI-12	SP	0.003
FRCI-12-SSP6-Q	FRCI-12	SP	0.003
FRCI-12-SSP1-10	FRCI-12	SP	10
FRCI-12-SSP12-10	FRCI-12	SP	10

* WP-Weak Plane; SP-Strong Plane (see Figure 11)

**-targeted stroke rate

***-defective specimens delaminated from the aluminum shear platen

Erroneous tests: LI-900-SWP4-Q

5. Uniaxial Strain Compression Test (Quasi-static Strain Rate)

The uniaxial strain compression (USC) (or "Compression-in a-box") test is designed to constrain radial strain while increasing the compressive axial load. The USC tests were performed using a die compaction test set-up as shown in Figure 16. The test set-up consists of a die, a punch, an LVDT to measure axial deformation of the specimen, and a total load load-cell to measure the axial load applied to the specimen (Figure 17). The frictional force between the specimen, the punch and the die-body and the lateral strain were not measured during the test, although the lateral strain was assumed to be zero consistent with the USC test configuration.

The cylindrical specimens were loaded along the axis of the cylinder and the lateral strain was suppressed effectively by a die-body creating a pseudo-uniaxial strain condition. The axial strain, ε_a, is measured as a function of the axial stress, σ_a. Since the lateral strains are effectively suppressed, ε_a is effectively equal to the volumetric strain, ε_v.

Figure 16. Uniaxial strain compression test set-up controlled by a servo-controlled system.
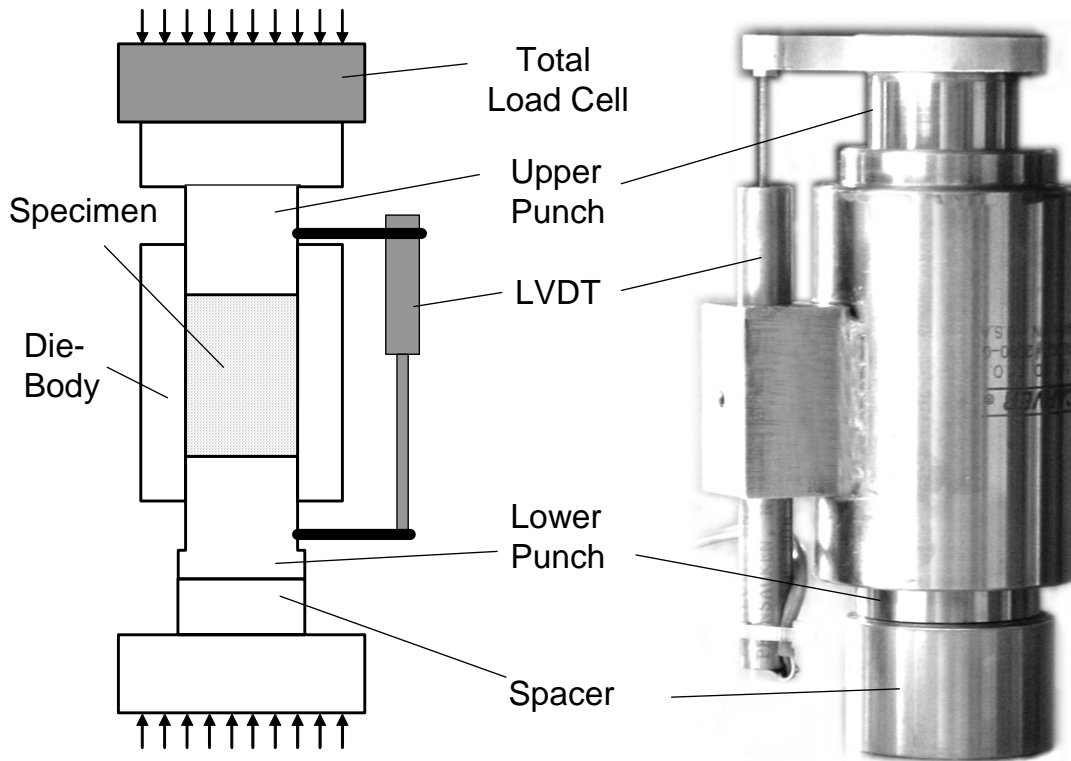
Figure 17.   A modified die compaction system with an LVDT to measure the axial displacement of the specimen for the "compression-in-a-box" test.

Right cylinder discs were used for the USC tests. Cylindrical cores were extracted from the TPS materials in IP and TTT orientations. The diameter of each specimen was nominally 1.125" to fit the bore of the die-body and the length of the specimens was 0.5". Both ends of the cores were ground flat within 0.005" tolerance. Thirty USC tests were conducted: five in the "through-the-thickness" orientation and five in the "in-plane" orientation for each TPS material. The detailed test-matrix is shown in Table 4 and the results are summarized in Appendix C, Table C1.

The specimen was inserted into the die-body and pushed to the bottom until it came into contact with the lower punch sitting on the spacer. The upper punch was lowered into the die-body until it contacted the specimen. Then, the LVDT attached to the die-body was zeroed with the end of the LVDT core in contact with the upper punch. The upper punch was lowered and the load was applied to the specimen at the targeted strain rate of 0.001 /s until the axial stress of about 100 psi was reached. Changes in specimen volume were calculated assuming the specimen could deform in the axial direction only, i.e., the die-body fully constrained the specimen in the radial direction.

Figures 18 and 19 show the axial stress-axial strain plots obtained in IP and TTT orientations, respectively. The stress-strain plot consists of three segments. The first segment is the elastic response of the material with a steep increase of σ_a up to the point when the specimen fails at the compressive strength corresponding to the confined condition.   The peak stress is usually

accompanied by a small stress drop (Figure 18) that may indicate a formation of compaction bands, a common phenomenon in porous materials (Olsson, 1999). The stress drop is conspicuous in specimens tested in the IP orientation. The next segment is crush, where the localized failure propagates throughout the specimen converting the intact material into compacted material with layers of compaction bands. This segment is characterized by an increase of ε_a up to about 0.7 without increasing the applied stress significantly. The last segment is the compaction of the material into a voidless state characterized by a rapid increase in the applied axial stress without significantly increasing ε_a.

Table 4. Compression-in-a-box test matrix for the Thermal Protection System (TPS) Materials.

Test ID	Material	Orientation[*]	Strain Rate[**] (1/s)
LI-900-BIP1-Q	LI-900	IP	0.001
LI-900-BIP2-Q	LI-900	IP	0.001
LI-900-BIP3-Q	LI-900	IP	0.001
LI-900-BIP4-Q	LI-900	IP	0.001
LI-900-BIP5-Q	LI-900	IP	0.001
LI-900-BT1-Q	LI-900	TTT	0.001
LI-900-BT2-Q	LI-900	TTT	0.001
LI-900-BT3-Q	LI-900	TTT	0.001
LI-900-BT4-Q	LI-900	TTT	0.001
LI-900-BT5-Q	LI-900	TTT	0.001
LI-2200-BIP1-Q	LI-2200	IP	0.001
LI-2200-BIP2-Q	LI-2200	IP	0.001
LI-2200-BIP3-Q	LI-2200	IP	0.001
LI-2200-BIP4-Q	LI-2200	IP	0.001
LI-2200-BIP6-Q	LI-2200	IP	0.001
LI-2200-BT1-Q	LI-2200	TTT	0.001
LI-2200-BT2-Q	LI-2200	TTT	0.001
LI-2200-BT3-Q	LI-2200	TTT	0.001
LI-2200-BT4-Q	LI-2200	TTT	0.001
LI-2200-BT5-Q	LI-2200	TTT	0.001
FRCI-12-BIP1-Q	FRCI-12	IP	0.001
FRCI-12-BIP2-Q	FRCI-12	IP	0.001
FRCI-12-BIP3-Q	FRCI-12	IP	0.001
FRCI-12-BIP4-Q	FRCI-12	IP	0.001
FRCI-12-BIP5-Q	FRCI-12	IP	0.001
FRCI-12-BT1-Q	FRCI-12	TTT	0.001
FRCI-12-BT2-Q	FRCI-12	TTT	0.001
FRCI-12-BT3-Q	FRCI-12	TTT	0.001
FRCI-12-BT4-Q	FRCI-12	TTT	0.001
FRCI-12-BT5-Q	FRCI-12	TTT	0.001

*-IP - "In-Plane"; TTT - "Through-The-thickness"
** - targeted strain rate.
LI-2200-BIP5-Q test was aborted due to a disconnection in the LVDT.

LI-900-BIP1-Q
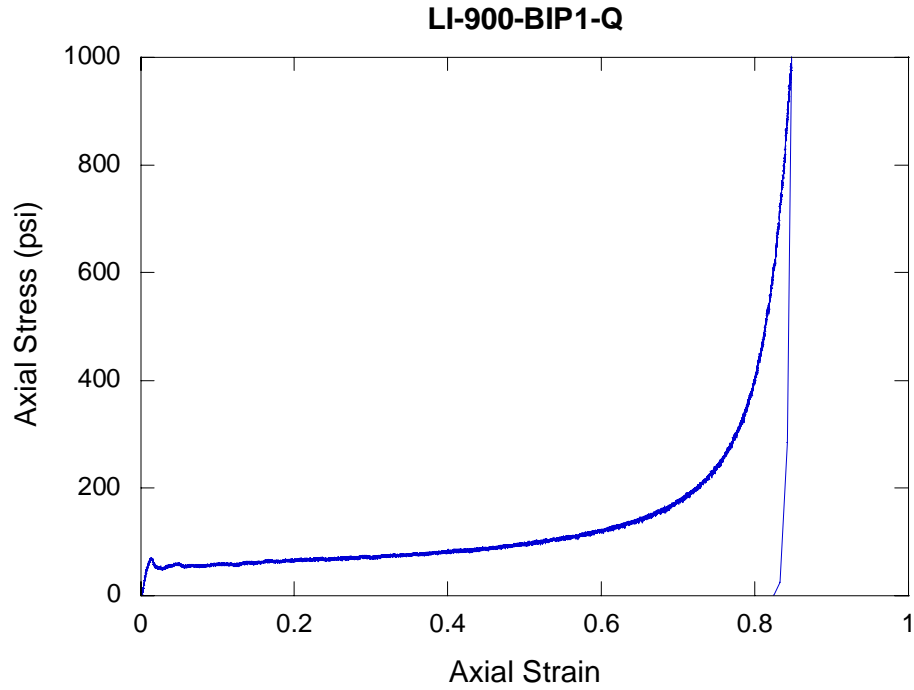
Figure 18. The axial stress versus axial strain curve obtained in USC testing of an LI-900 material loaded in the "in-plane" orientation.

LI-900-BT1-Q
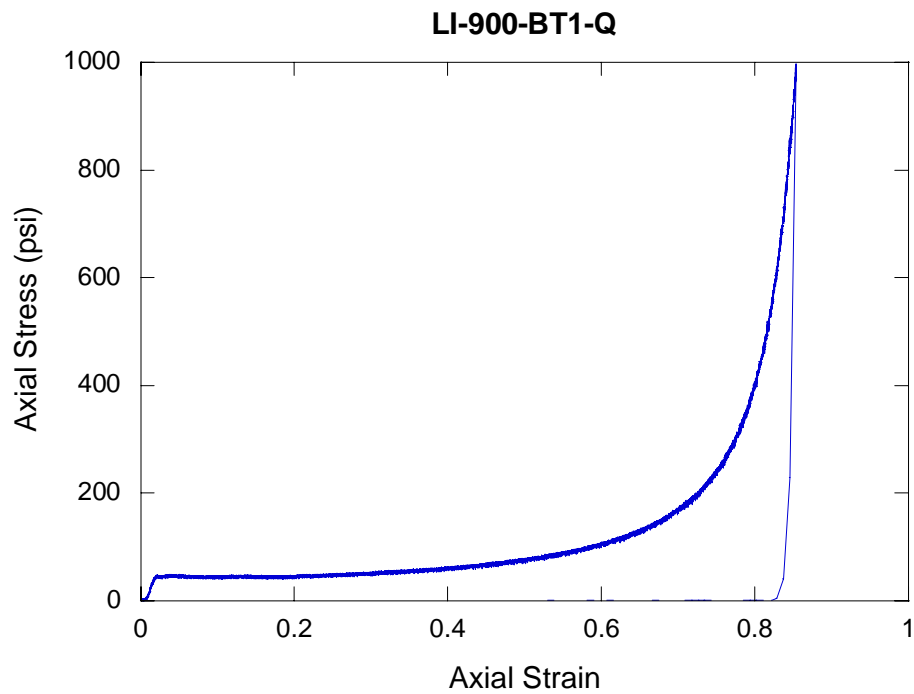
Figure 19. The axial stress versus axial strain curve obtained in USC testing of an LI-900 material loaded in the "through-the-thickness" orientation.

6. Split Hopkinson Pressure Bar Test (Dynamic Strain Rate)

To investigate the dynamic behavior of the TPS materials under unconfined and confined uniaxial compressive stress conditions, the Split Hopkinson Pressure Bar (SHPB or Kolsky bar) was used (Kolsky, 1949). Figure 20 show the SHPB set-up with a calibrating load cell and a data acquisition system. The SHPB set-up consists of a striker bar, an incident bar and a transmission bar made from an aluminum alloy, AL7075-T6. In addition, a titanium confinement ring was placed over the specimen when the confined SHPB testing was conducted (Figure 21).

The incident and the transmission bars were instrumented with strain gages to capture elastic waves generated by the striker bar colliding with the incident bar. Foil type strain gages were used in the incident bar and semiconductor strain gages were used in the transmission bar. Use of semiconductor strain gages allows us to record the acoustic wave transmitted to the transmission bar due to low acoustic impedance of the TPS materials. The semiconductor strain gages were calibrated using a load cell mounted in place of the specimen (Figure 20).

A disk-shaped specimen (1.00" in diameter and 0.25" in length) was placed between the incident and the transmission bars and the striker bar was launched by compressed air. An oscilloscopic data acquisition system simultaneously captured the wavelets in the incident and the transmission bars at a rate of 2.5×10^6 sample/s per channel.
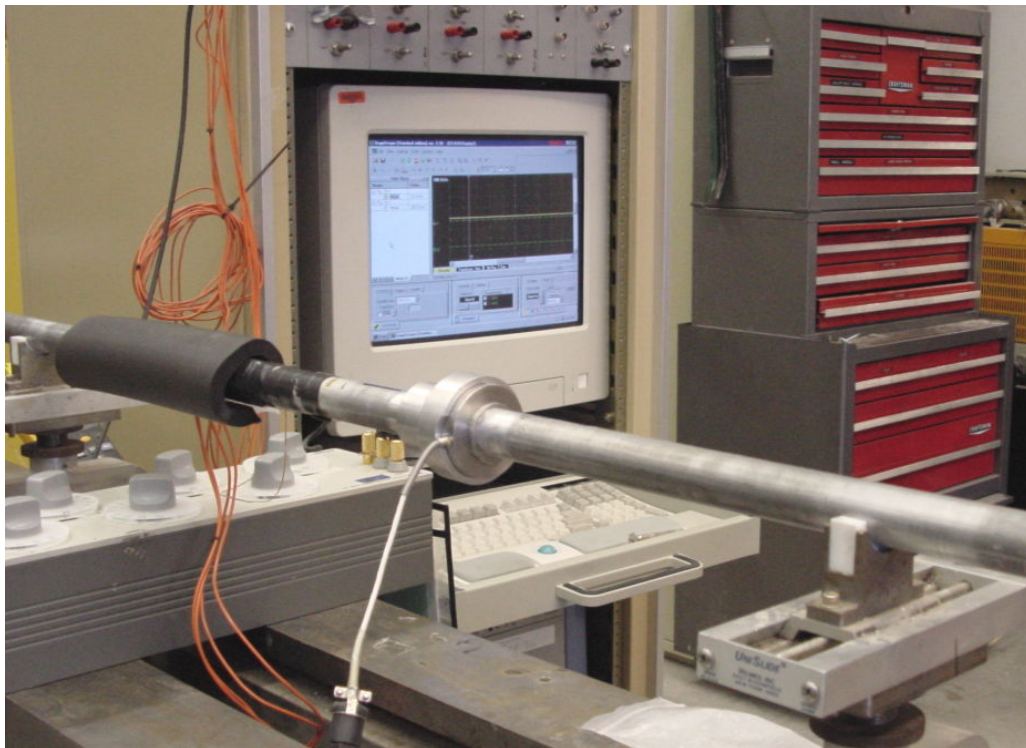
Figure 20. Split Hopkinson pressure bar set-up with a calibrating load cell.
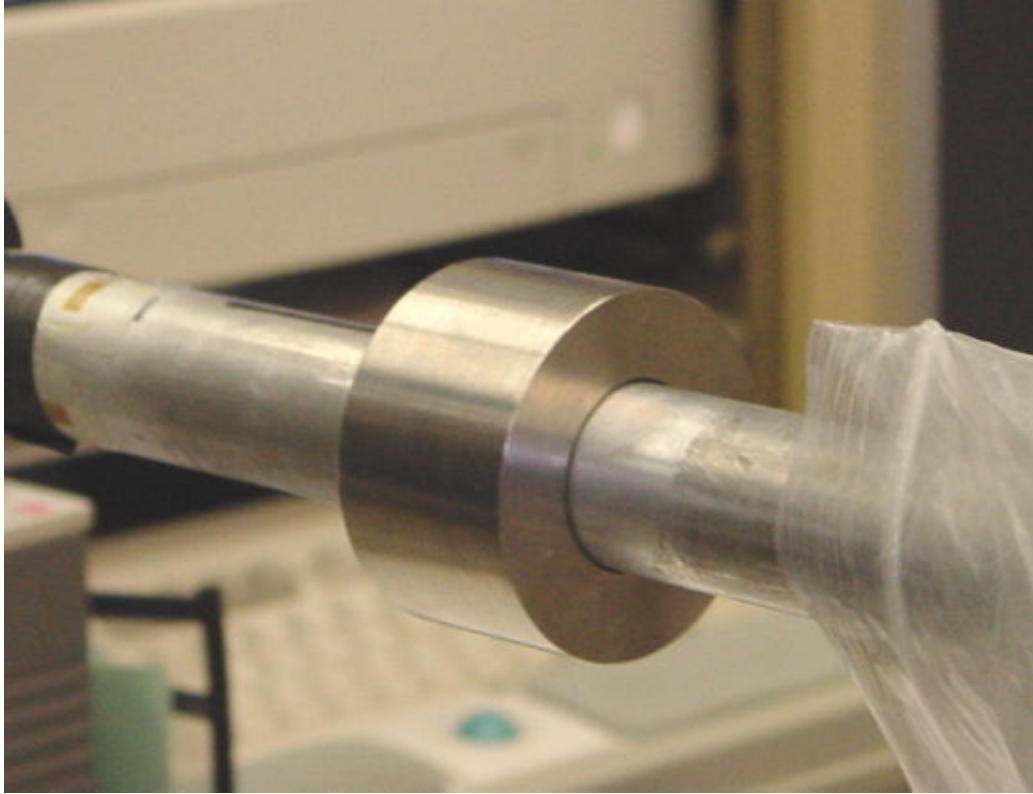
Figure 21. Split Hopkinson pressure bar set-up with a lateral confinement ring installed over the specimen.

When the striker bar impacts the incident bar, an elastic wave is generated and travels through the incident bar. When the elastic wave reached the interface (interface **a** in Figure 22) between the incident bar and the specimen, a fraction of the wave is reflected back into the incident bar due to the impedance mismatch between the sample and the bar. The remainder of the wave travels through the specimen and reaches the interface (interface **b** in Figure 22) between the specimen and the transmission bar. Based on one dimensional theory of elastic wave propagation in a bar and the continuity of displacement and stress equilibrium at the interface, the following equations can be derived to describe stress, strain and strain rate in the specimen (Kolsky, 1949):

$$\sigma_a = E\frac{A}{A_s}(\varepsilon_i + \varepsilon_r)$$

$$\sigma_b = E\frac{A}{A_s}(\varepsilon_t)$$

$$\dot{\varepsilon} = -\frac{2V_l}{L}\varepsilon_r$$

$$\varepsilon = \frac{2V_l}{L} \int_0^t \varepsilon_r \, dt$$

where σ_a is the stress in the interface between the sample and the incident bar; σ_b is the stress in the interface between the sample and the transmission bar; E is the modulus of the transmission bar; A is the cross-sectional area of the transmission bar; A_s is the cross-sectional area of the specimen; ε_i, ε_r, and ε_t are the incident, reflected, and transmitted strains, respectively; $\dot{\varepsilon}$ is the strain rate in the specimen; V_l is the longitudinal wave velocity in the incident bar; L is the initial length of the specimen; and t is time. The test parameters used for the TPS materials testing are listed in Table 5.
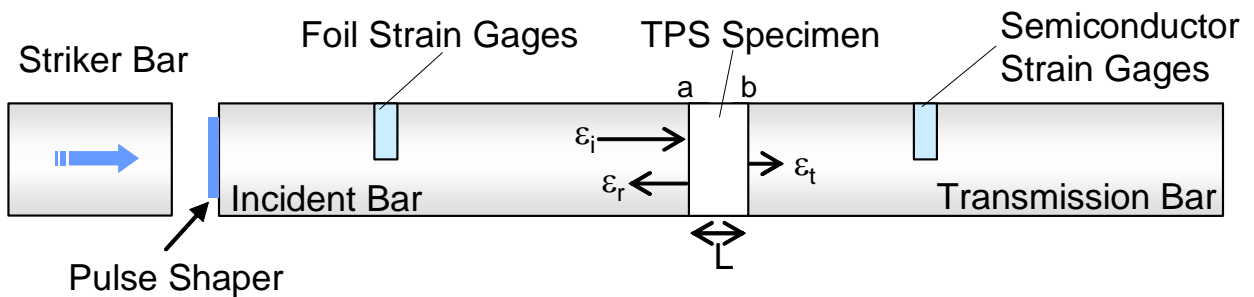
Figure 22. Schematic of the split Hopkinson pressure bar experimental set-up and the elastic waves in the bar-specimen interfaces.

Table 5. Test parameters used for SHPB testing of Thermal Protection System (TPS) materials.

SHPB test parameter	Constant Value
Cross-sectional area of the transmission bar, A	1.00 inch^2
Cross-sectional area of the specimen, A$_s$	1.00 inch^2
Initial length of the specimen, L	0.25 inch
Longitudinal wave velocity in AL7075-T6 bar, V_l	196,732 inch/s
Young's modulus of AL7075-T6, E	10,440,000 psi
Strain sensitivity in the incident bar	32,395 μstrain/V
Strain sensitivity in the transmission bar	634 μstrain/V

In order to achieve a dynamic equilibrium of stress and a homogeneous deformation throughout the specimen, the stress wave at the incident bar interface should rise gradually through pulse shaping. Figure 23 shows a pulse shaping disk attached to the end of the incident bar. When the striker bar impacts the pulse shaper, a thin disk of felt metal deforms plastically to generate a monotonically rising pulse with a longer period. Before the peak stress in the incident bar is reached, the elastic wave travels between interfaces **a** and **b** several times to achieve a dynamic

equilibrium of stress and a homogeneous deformation in the specimen. Figure 24 shows a typical record from SHPB testing of a TPS specimen. Shown are the strain gage records for the incident wave, ε_i reflected wave, ε_r and the transmitted wave, ε_t. Based on the SHPB equations listed above, stress and strain rate of the specimen under dynamic loading can be calculated with respect to strain (Figure 25). From the stress-strain plot, the peak stress was obtained to estimate the strength of the TPS material. The strain rate for the peak stress can be picked from the same plot (Figure 25). The results of SHPB testing of the TPS materials are summarized in Appendix D, Tables D1 through D3.
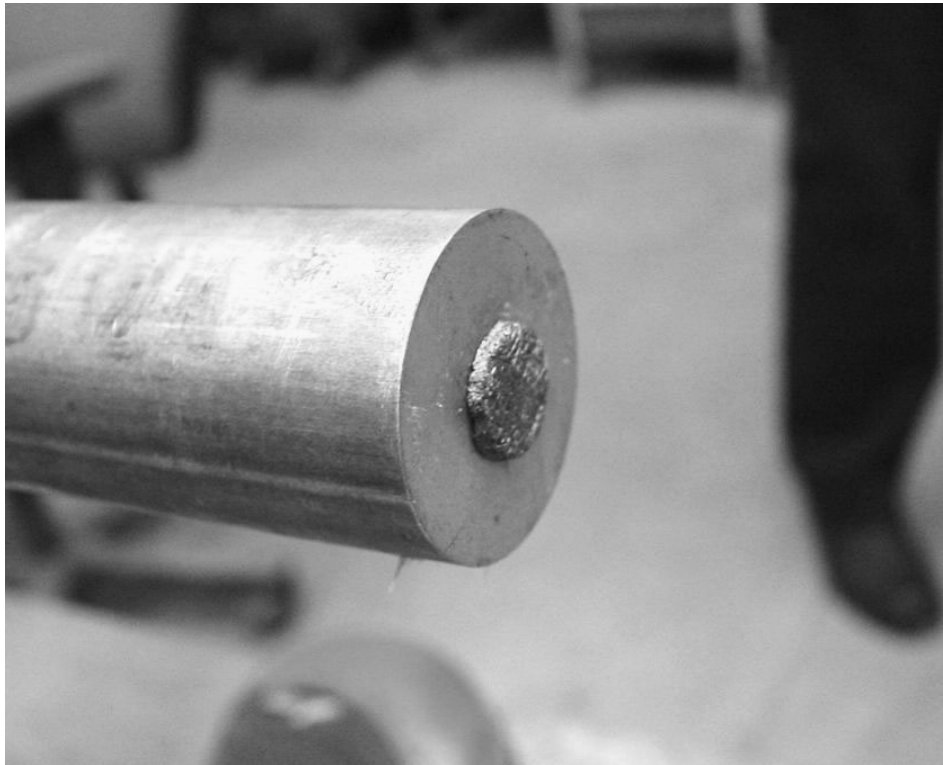
Figure 23. A pulse shaper disk made out of a felt metal attached to the end of the incident bar of the split Hopkinson pressure bar where the striker bar impacts the incident bar.
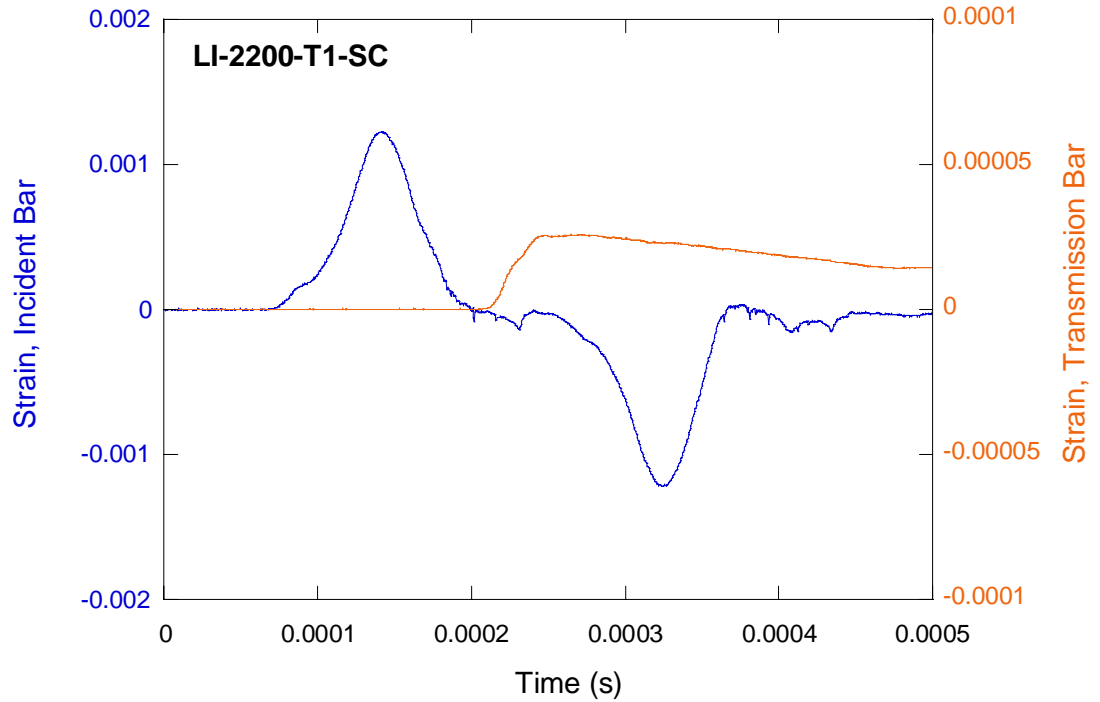
Figure 24. Typical record obtained during SHPB testing of an LI-2200 specimen.
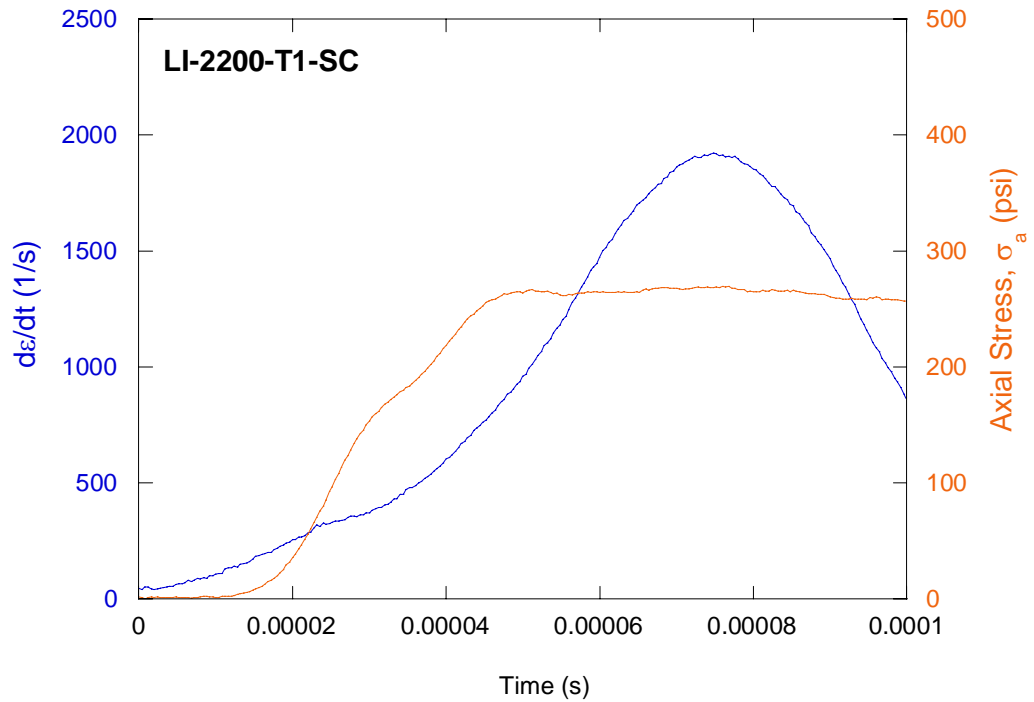
Figure 25. Typical stress – strain and strain rate-strain plots obtained during SHPB testing of an LI-2200 specimen.

7. Summary and Conclusions

An experimental study was conducted to measure the mechanical properties of the Thermal Protection System (TPS) materials used for the Space Shuttle. Three types of TPS materials (LI-900, LI-2200, and FRCI-12) were tested in "in-plane" and "out-of-plane" orientations. Four types of quasi-static mechanical tests (uniaxial tension, uniaxial compression, uniaxial strain, and shear) were performed under low (10^{-4} to 10^{-3}/s) and intermediate (1 to 10/s) strain rate conditions. In addition, split Hopkinson pressure bar tests were conducted to obtain the strength of the materials under a relatively higher strain rate (~10^2 to 10^3/s) condition. For each TPS material the results are presented in Appendices A through E as functions of loading type, loading orientation, and applied strain rate

The comparative trends and values of strength, Young's modulus, and shear modulus under different strain rates are presented in Appendix E in graphical form. In general, TPS materials have higher strength and higher Young's modulus when tested in "in-plane" compared to "through-the-thickness" orientations under compressive (unconfined and confined) and tensile stress conditions. In both stress conditions, the strength of the material increases as the strain rate increases. The rate of increase in LI-900 is relatively small compared to those for the other two TPS materials tested in this study. But, the Young's modulus appears to be insensitive to the different strain rates applied.

The FRCI-12 material, designed to replace the heavier LI-2200, showed higher strengths under tensile and shear stress conditions. But, under a compressive stress condition, LI-2200 showed higher strength than FRCI-12. As far as the modulus is concerned, LI-2200 has higher Young's modulus both in compression and in tension. The shear modulus of FRCI-12 and LI-2200 fell in the same range.

References

Kolsky, H., An Investigation of the Mechanical Properties of Materials at Very High Rates of Strain, Proc. Roy. Phys. Soc., B62, 676-700, 1949.

NASA, NSTS (National Space Transportation System) Shuttle Reference Manual, 1988.

Olsson, W. A., Theoretical and experimental investigation of compaction band in porous rock, J. Geophys. Res., 104, 7219-7228, 1999.

Slenk J., Dynamic Properties Testing Of TPS Materials Tested at Sandia National Laboratories, Detailed Test Plan, Boeing Thermal Management Systems Material & Process Engineering Huntington Beach/Seal Beach Host Engineering, 2004.

Slenk J., Personal communication, 2005.

Appendix A

Summary of Uniaxial Tension and Compression Test Results

Table A1. Summary of uniaxial compression and tension tests for LI-900.

Test ID	Material	Test Type	Orientation	Strain Rate (1/s)	Peak Stress* (psi)	Young's Modulus (psi)
LI-900-CIP1-Q	LI-900	UC	IP	0.0007	85	23980
LI-900-CIP2-Q	LI-900	UC	IP	0.0008	89	22920
LI-900-CIP3-Q	LI-900	UC	IP	0.0009	60	21450
LI-900-CIP4-Q	LI-900	UC	IP	0.0008	73	24820
LI-900-CIP5-Q	LI-900	UC	IP	0.0008	109	23930
LI-900-CIP6-10	LI-900	UC	IP	2.2	84	16860
LI-900-CIP7-10	LI-900	UC	IP	2.1	92	17200
LI-900-CIP8-10	LI-900	UC	IP	1.9	112	24530
LI-900-CIP9-10	LI-900	UC	IP	2.0	102	22080
LI-900-CIP10-10	LI-900	UC	IP	2.0	102	21870
LI-900-CT1R-Q**	LI-900	UC	TTT	0.0011	47	4260
LI-900-CT2-Q	LI-900	UC	TTT	0.0009	57	7230
LI-900-CT3-Q	LI-900	UC	TTT	0.0009	54	7910
LI-900-CT4-Q	LI-900	UC	TTT	0.0009	52	7170
LI-900-CT5-Q	LI-900	UC	TTT	0.0008	51	7960
LI-900-CT6-10	LI-900	UC	TTT	2.7	68	7810
LI-900-CT7-10	LI-900	UC	TTT	2.7	64	9210
LI-900-CT8-10	LI-900	UC	TTT	2.9	63	5880
LI-900-CT9-10	LI-900	UC	TTT	2.6	70	8960
LI-900-IP1-Q	LI-900	UT	IP	-0.0007	-56	27550
LI-900-IP2-Q	LI-900	UT	IP	-0.0007	-71	29130
LI-900-IP3-Q	LI-900	UT	IP	-0.0008	-69	27400
LI-900-IP4-Q	LI-900	UT	IP	-0.0006	-70	37820
LI-900-IP5-Q	LI-900	UT	IP	-0.0008	-75	27340
LI-900-IP7-10	LI-900	UT	IP	-2.0	-102	29370
LI-900-IP8-10	LI-900	UT	IP	-1.7	-61	36760
LI-900-IP9-10	LI-900	UT	IP	-1.8	-98	30950
LI-900-IP10-10	LI-900	UT	IP	-1.8	-96	26100
LI-900-IP12-10	LI-900	UT	IP	-2.0	-91	23640
LI-900-T1-Q	LI-900	UT	TTT	-0.0010	-34	8760
LI-900-T2-Q	LI-900	UT	TTT	-0.0011	-40	8000
LI-900-T3-Q	LI-900	UT	TTT	-0.0010	-30	6020
LI-900-T4-Q	LI-900	UT	TTT	-0.0011	-28	5730
LI-900-T5-Q	LI-900	UT	TTT	-0.0009	-31	8610
LI-900-T7-10	LI-900	UT	TTT	-3.0	-46	7010
LI-900-T8-10	LI-900	UT	TTT	-2.2	-43	7240
LI-900-T9-10	LI-900	UT	TTT	-2.0	-49	8860
LI-900-T10-10	LI-900	UT	TTT	-2.3	-47	7860
LI-900-T11-10	LI-900	UT	TTT	-3.3	-56	11670

UC-Uniaxial Compression; UT-Uniaxial Tension

IP-"In-Plane"; TTT-"Through-The-Thickness"

*-sign convention (compressive stress and corresponding strain in stress direction are positive.)
**-Sandia prepared specimen from LI-900 block for SHPB testing. The material may not be consistent with other specimens tested under the same condition.

Table A2. Summary of uniaxial compression and tension tests for LI-2200.

Test ID	Material	Test Type	Orientation	Strain Rate (1/s)	Peak Stress* (psi)	Young's Modulus (psi)
LI-2200-CIP1-Q	LI-2200	UC	IP	0.0010	332	71150
LI-2200-CIP2-Q	LI-2200	UC	IP	0.0008	335	78540
LI-2200-CIP3-Q	LI-2200	UC	IP	0.0008	332	76670
LI-2200-CIP4-Q	LI-2200	UC	IP	0.0008	325	72260
LI-2200-CIP5-Q	LI-2200	UC	IP	0.0009	297	76860
LI-2200-CIP6-10	LI-2200	UC	IP	2.9	383	81720
LI-2200-CIP7-10	LI-2200	UC	IP	2.7	380	88280
LI-2200-CIP8-10	LI-2200	UC	IP	2.7	370	81910
LI-2200-CIP9-10	LI-2200	UC	IP	2.4	364	86140
LI-2200-CIP10-10	LI-2200	UC	IP	2.7	319	85820
LI-2200-CT1-Q	LI-2200	UC	TTT	0.0010	189	24060
LI-2200-CT2-Q	LI-2200	UC	TTT	0.0009	181	26410
LI-2200-CT3-Q	LI-2200	UC	TTT	0.0009	178	26770
LI-2200-CT4-Q	LI-2200	UC	TTT	0.0009	190	22920
LI-2200-CT5-Q	LI-2200	UC	TTT	0.0010	190	26200
LI-2200-CT6-10	LI-2200	UC	TTT	3.5	226	24260
LI-2200-CT7-10	LI-2200	UC	TTT	3.5	221	24650
LI-2200-CT8-10	LI-2200	UC	TTT	3.5	226	22860
LI-2200-CT9-10	LI-2200	UC	TTT	3.6	248	24280
LI-2200-CT10-10	LI-2200	UC	TTT	3.6	239	21760
LI-2200-IP1-Q	LI-2200	UT	IP	-0.0005	-130	84720
LI-2200-IP3-Q	LI-2200	UT	IP	-0.0005	-156	92210
LI-2200-IP4-Q	LI-2200	UT	IP	-0.0005	-72	83350
LI-2200-IP11-Q	LI-2200	UT	IP	-0.0004	-77	81410
LI-2200-IP12-Q	LI-2200	UT	IP	-0.0005	-118	85510
LI-2200-IP6-10	LI-2200	UT	IP	-1.2	-189	120590
LI-2200-IP7-10	LI-2200	UT	IP	-1.0	-200	111220
LI-2200-IP8-10	LI-2200	UT	IP	-1.4	-175	78600
LI-2200-IP9-10	LI-2200	UT	IP	-1.6	-157	99190
LI-2200-IP10-10	LI-2200	UT	IP	-1.3	-153	79800
LI-2200-T1-Q	LI-2200	UT	TTT	-0.0007	-67	30970
LI-2200-T2-Q	LI-2200	UT	TTT	-0.0007	-69	25870
LI-2200-T3-Q**	LI-2200	UT	TTT	NA	-12	NA
LI-2200-T4-Q	LI-2200	UT	TTT	-0.0007	-61	26730
LI-2200-T5-Q	LI-2200	UT	TTT	-0.0006	-37	26000
LI-2200-T7-10	LI-2200	UT	TTT	-1.3	-94	27560
LI-2200-T8-10	LI-2200	UT	TTT	-1.9	-106	38710
LI-2200-T9-10	LI-2200	UT	TTT	-1.9	-105	30250
LI-2200-T10-10	LI-2200	UT	TTT	-1.8	-111	25820
LI-2200-T13-10	LI-2200	UT	TTT	-0.4	-54	79360

UC-Uniaxial Compression; UT-Uniaxial Tension

IP-"In-Plane"; TTT-"Through-The-Thickness"

*-sign convention (compressive stress and corresponding strain in stress direction are positive.)

**-Erroneous test

Table A3. Summary of uniaxial compression and tension tests for FRCI-12.

Test ID	Material	Test Type	Orientation	Strain Rate (1/s)	Peak Stress* (psi)	Young's Modulus (psi)
FRCI-12-CIP1-Q	FRCI-12	UC	IP	0.0008	263	55110
FRCI-12-CIP2-Q	FRCI-12	UC	IP	0.0009	267	44570
FRCI-12-CIP3-Q	FRCI-12	UC	IP	0.0009	230	40490
FRCI-12-CIP4-Q	FRCI-12	UC	IP	0.0010	222	33870
FRCI-12-CIP5-Q	FRCI-12	UC	IP	0.0009	275	53930
FRCI-12-CIP6-10	FRCI-12	UC	IP	3.2	271	34820
FRCI-12-CIP9-10	FRCI-12	UC	IP	2.9	317	49780
FRCI-12-CIP10-10	FRCI-12	UC	IP	3.1	306	39920
FRCI-12-CIP13-10	FRCI-12	UC	IP	2.8	318	48910
FRCI-12-CT1-Q	FRCI-12	UC	TTT	0.0010	154	8580
FRCI-12-CT2-Q	FRCI-12	UC	TTT	0.0010	150	9390
FRCI-12-CT3-Q	FRCI-12	UC	TTT	0.0009	144	9330
FRCI-12-CT4-Q	FRCI-12	UC	TTT	0.0010	137	8800
FRCI-12-CT5-Q	FRCI-12	UC	TTT	0.0009	133	8780
FRCI-12-CT6-10	FRCI-12	UC	TTT	3.8	172	8650
FRCI-12-CT7-10	FRCI-12	UC	TTT	3.6	173	9070
FRCI-12-CT8-10	FRCI-12	UC	TTT	3.9	186	9170
FRCI-12-CT9-10	FRCI-12	UC	TTT	3.7	194	9460
FRCI-12-CT10-10	FRCI-12	UC	TTT	3.6	165	8590
FRCI-12-IP2-Q	FRCI-12	UT	IP	-0.0008	-231	49960
FRCI-12-IP3-Q	FRCI-12	UT	IP	-0.0007	-224	52920
FRCI-12-IP4-Q	FRCI-12	UT	IP	-0.0007	-216	54640
FRCI-12-IP5-Q	FRCI-12	UT	IP	-0.0007	-268	58260
FRCI-12-IP11-Q	FRCI-12	UT	IP	-0.0008	-219	48880
FRCI-12-IP6-10	FRCI-12	UT	IP	-2.8	-378	53480
FRCI-12-IP7-10	FRCI-12	UT	IP	-2.1	-286	64050
FRCI-12-IP8-10	FRCI-12	UT	IP	-3.0	-286	43110
FRCI-12-IP9-10	FRCI-12	UT	IP	-2.3	-387	63670
FRCI-12-IP10-10	FRCI-12	UT	IP	-2.2	-353	65590
FRCI-12-T1-Q	FRCI-12	UT	TTT	-0.001	-76	10540
FRCI-12-T2-Q	FRCI-12	UT	TTT	-0.001	-85	10250
FRCI-12-T3-Q	FRCI-12	UT	TTT	-0.001	-80	9820
FRCI-12-T4-Q	FRCI-12	UT	TTT	-0.001	-76	9660
FRCI-12-T5-Q	FRCI-12	UT	TTT	-0.001	-81	9590
FRCI-12-T6-10	FRCI-12	UT	TTT	-4.0	-110	9690
FRCI-12-T7-10	FRCI-12	UT	TTT	-4.2	-125	10400
FRCI-12-T8-10	FRCI-12	UT	TTT	-3.9	-307	28030
FRCI-12-T9-10	FRCI-12	UT	TTT	-3.7	-281	29320
FRCI-12-T10-10	FRCI-12	UT	TTT	-3.8	-313	31380

UC-Uniaxial Compression; UT-Uniaxial Tension

IP-"In-Plane"; TTT-"Through-The-Thickness"

*-sign convention (compressive stress and corresponding strain in stress direction are positive.)

Appendix B

Summary of Shear Test Results

Table B1. Summary of shear test results for LI-900

Test ID	Material	Test Type	Orientation	Strain Rate, $d\gamma_{xy}/dt$ (1/s)	Peak Stress, σ_{xy} (psi)	Shear Modulus, G (psi)
LI-900-SSP1-Q	LI-900	Shear	SP	0.002	60	8280
LI-900-SSP2-Q	LI-900	Shear	SP	0.003	58	7300
LI-900-SSP3-Q*	LI-900	Shear	SP	0.002	43	7870
LI-900-SSP4-Q	LI-900	Shear	SP	0.003	56	7586
LI-900-SSP5-Q	LI-900	Shear	SP	0.003	58	7330
LI-900-SSP105-Q[#]	LI-900	Shear	SP	0.002	55	9890
LI-900-SSP6-10*	LI-900	Shear	SP	6.3	53	9070
LI-900-SSP7-10	LI-900	Shear	SP	3.2	83	16870
LI-900-SSP8-10*	LI-900	Shear	SP	5.2	54	10730
LI-900-SSP9-10*	LI-900	Shear	SP	5.2	52	11110
LI-900-SSP10-10*	LI-900	Shear	SP	5.6	59	10850
LI-900-SSP101-10[#]	LI-900	Shear	SP	4.7	62	12280
LI-900-SSP102-10[#]	LI-900	Shear	SP	4.7	69	12690
LI-900-SSP103-10[#]	LI-900	Shear	SP	4.9	75	13670
LI-900-SSP104-10[#]	LI-900	Shear	SP	4.8	75	14300
LI-900-SWP1-Q	LI-900	Shear	WP	0.003	46	5580
LI-900-SWP2-Q	LI-900	Shear	WP	0.003	40	5300
LI-900-SWP3-Q	LI-900	Shear	WP	0.003	42	4950
LI-900-SWP5-Q	LI-900	Shear	WP	0.003	44	5010
LI-900-SWP6-Q	LI-900	Shear	WP	0.003	40	5050
LI-900-SWP7-10	LI-900	Shear	WP	6.8	44	6390
LI-900-SWP8-10	LI-900	Shear	WP	7.5	49	5970
LI-900-SWP9-10	LI-900	Shear	WP	7.8	46	5400
LI-900-SWP10-10	LI-900	Shear	WP	7.9	49	5970
LI-900-SWP11-10	LI-900	Shear	WP	7.5	49	6460

WP-Weak Plane; SP-Strong Plane (see Figure 11)

Shear Modulus, G is calculated by the shear stress σ_{xy} divided by the engineering shear strain $\gamma_{xy}(=2^*\varepsilon_{xy})$

*Defective specimens. Disregard the results.

[#]Sandia prepared specimens.

Table B2. Summary of shear test results for LI-2200

Test ID	Material	Test Type	Orientation	Strain Rate, $d\gamma_{xy}/dt$ (1/s)	Peak Stress, σ_{xy} (psi)	Shear Modulus, G (psi)
LI-2200-SSP1-Q	LI-2200	Shear	SP	0.002	106	20230
LI-2200-SSP2-Q	LI-2200	Shear	SP	0.002	64	15720
LI-2200-SSP3-Q	LI-2200	Shear	SP	0.0015	88	21390
LI-2200-SSP4-Q	LI-2200	Shear	SP	0.002	68	12030
LI-2200-SSP5-Q	LI-2200	Shear	SP	0.002	111	21320
LI-2200-SSP6-10	LI-2200	Shear	SP	4.7	107	19830
LI-2200-SSP9-10	LI-2200	Shear	SP	3.6	153	29432
LI-2200-SWP1-Q	LI-2200	Shear	WP	0.001	84	18560
LI-2200-SWP2-Q	LI-2200	Shear	WP	0.001	97	21330
LI-2200-SWP4-Q	LI-2200	Shear	WP	0.001	108	23520
LI-2200-SWP5-Q	LI-2200	Shear	WP	0.002	86	17820
LI-2200-SWP11-Q	LI-2200	Shear	WP	0.002	104	20230
LI-2200-SWP7-10	LI-2200	Shear	WP	4.1	119	20820
LI-2200-SWP8-10	LI-2200	Shear	WP	4.2	110	21490
LI-2200-SWP9-10	LI-2200	Shear	WP	3.9	110	20940
LI-2200-SWP10-10	LI-2200	Shear	WP	3.7	132	24140
LI-2200-SWP12-10	LI-2200	Shear	WP	4.6	125	20040

WP-Weak Plane; SP-Strong Plane (see Figure 11)

Shear Modulus, G is calculated by the shear stress σ_{xy} divided by the engineering shear strain $\gamma_{xy}(=2*\varepsilon_{xy})$

Defective specimens : LI-2200-SSP7-10, LI-2200-SSP8-10, and LI-2200-SSP10-10

Table B3. Summary of shear test results for FRCI-12

Test ID	Material	Test Type	Orientation	Strain Rate, $d\gamma_{xy}/dt$ (1/s)	Peak Stress, σ_{xy} (psi)	Shear Modulus, G (psi)
FRCI-12-SSP2-Q	FRCI-12	Shear	SP	0.002	187	20630
FRCI-12-SSP3-Q	FRCI-12	Shear	SP	0.002	158	18170
FRCI-12-SSP4-Q	FRCI-12	Shear	SP	0.002	161	17980
FRCI-12-SSP5-Q	FRCI-12	Shear	SP	0.0015	195	25650
FRCI-12-SSP6-Q	FRCI-12	Shear	SP	0.002	179	23260
FRCI-12-SSP1-10	FRCI-12	Shear	SP	5.5	152	15610
FRCI-12-SSP12-10	FRCI-12	Shear	SP	4.9	181	21060
FRCI-12-SWP1-Q	FRCI-12	Shear	WP	0.003	101	8330
FRCI-12-SWP2-Q	FRCI-12	Shear	WP	0.003	116	9160
FRCI-12-SWP3-Q	FRCI-12	Shear	WP	0.003	120	9130
FRCI-12-SWP4-Q	FRCI-12	Shear	WP	0.003	111	8710
FRCI-12-SWP5-Q	FRCI-12	Shear	WP	0.003	112	8700
FRCI-12-SWP12-10	FRCI-12	Shear	WP	12	148	11280
FRCI-12-SWP13-10	FRCI-12	Shear	WP	6.8	149	8940

WP-Weak Plane; SP-Strong Plane (see Figure 11)

Shear Modulus, G is calculated by the shear stress σ_{xy} divided by the engineering shear strain $\gamma_{xy}(=2*\varepsilon_{xy})$

Appendix C

Summary of Uniaxial Strain Compression (or "Compression-in-a-box") Test Results

Table C1. Summary of uniaxial strain compression (or "Compression-in-a-box") tests for the Thermal Protection System (TPS) materials.

Test ID	Material	Orientation	Strain Rate, $d\varepsilon_a/dt$ (1/s)	Failure Stress (psi)
LI-900-BIP1-Q	LI-900	IP	0.001	69
LI-900-BIP2-Q	LI-900	IP	0.001	70
LI-900-BIP3-Q	LI-900	IP	0.001	73
LI-900-BIP4-Q	LI-900	IP	0.001	70
LI-900-BIP5-Q	LI-900	IP	0.001	77
LI-900-BT1-Q	LI-900	TTT	0.001	47
LI-900-BT2-Q	LI-900	TTT	0.001	46
LI-900-BT3-Q	LI-900	TTT	0.001	44
LI-900-BT4-Q	LI-900	TTT	0.001	43
LI-900-BT5-Q	LI-900	TTT	0.001	44
LI-2200-BIP1-Q	LI-2200	IP	0.001	318
LI-2200-BIP2-Q	LI-2200	IP	0.001	313
LI-2200-BIP3-Q	LI-2200	IP	0.001	329
LI-2200-BIP4-Q	LI-2200	IP	0.001	324
LI-2200-BIP6-Q	LI-2200	IP	0.001	311
LI-2200-BT1-Q	LI-2200	TTT	0.001	141
LI-2200-BT2-Q	LI-2200	TTT	0.001	144
LI-2200-BT3-Q	LI-2200	TTT	0.001	156
LI-2200-BT4-Q	LI-2200	TTT	0.001	168
LI-2200-BT5-Q	LI-2200	TTT	0.001	146
FRCI-12-BIP1-Q	FRCI-12	IP	0.001	298
FRCI-12-BIP2-Q	FRCI-12	IP	0.001	298
FRCI-12-BIP3-Q	FRCI-12	IP	0.001	300
FRCI-12-BIP4-Q	FRCI-12	IP	0.001	290
FRCI-12-BIP5-Q	FRCI-12	IP	0.001	283
FRCI-12-BT1-Q	FRCI-12	TTT	0.001	115
FRCI-12-BT2-Q	FRCI-12	TTT	0.001	119
FRCI-12-BT3-Q	FRCI-12	TTT	0.001	126
FRCI-12-BT4-Q	FRCI-12	TTT	0.001	128
FRCI-12-BT5-Q	FRCI-12	TTT	0.001	129

IP-"In-Plane"; TTT-"Through-The-Thickness"
ε_a-axial strain

Appendix D

Summary of Split Hopkinson Pressure Bar Test Results

Table D1. Summary of split Hopkinson pressure bar testing of LI-900.

Test ID	Material	Orientation	Confinement	Strain rate at failure (1/s)	Strain rate average (1/s)	Peak stress (psi)
LI-900-IP1-SU	LI-900	IP	Laterally unconstrained	712	247	96
LI-900-IP2-SU	LI-900	IP	Laterally unconstrained	565	215	101
LI-900-IP3-SU	LI-900	IP	Laterally unconstrained	765	287	97
LI-900-IP4-SU	LI-900	IP	Laterally unconstrained	864	282	91
LI-900-IP5-SU	LI-900	IP	Laterally unconstrained	724	259	95
LI-900-IP1-SC	LI-900	IP	Laterally constrained	613	259	96
LI-900-IP2-SC	LI-900	IP	Laterally constrained	802	318	93
LI-900-IP3-SC	LI-900	IP	laterally constrained	827	254	100
LI-900-IP4-SC	LI-900	IP	Laterally constrained	872	272	94
LI-900-IP5-SC	LI-900	IP	Laterally constrained	815	324	95
LI-900-T1-SU	LI-900	TTT	Laterally unconstrained	637	264	64
LI-900-T2-SU	LI-900	TTT	Laterally unconstrained	823	324	67
LI-900-T3-SU	LI-900	TTT	Laterally unconstrained	894	299	63
LI-900-T4-SU	LI-900	TTT	Laterally unconstrained	918	322	66
LI-900-T5-SU	LI-900	TTT	Laterally unconstrained	1014	313	64
LI-900-T1-SC	LI-900	TTT	Laterally constrained	899	280	65
LI-900-T2-SC	LI-900	TTT	Laterally constrained	932	309	60
LI-900-T3-SC	LI-900	TTT	Laterally constrained	1062	371	61
LI-900-T4-SC	LI-900	TTT	Laterally constrained	1036	327	62
LI-900-T5-SC	LI-900	TTT	Laterally constrained	1047	342	62

IP-"In-Plane"; TTT-"Through-The-Thickness"

Table D2. Summary of split Hopkinson pressure bar testing of LI-2200.

Test ID	Material	Orientation	Confinement	Strain rate at failure (1/s)	Strain rate average (1/s)	Peak stress (psi)
LI-2200-IP1-SU	LI-2200	IP	Laterally unconstrained	1173	412	433
LI-2200-IP2-SU	LI-2200	IP	Laterally unconstrained	1061	428	448
LI-2200-IP3-SU	LI-2200	IP	Laterally unconstrained	1053	369	481
LI-2200-IP4-SU	LI-2200	IP	Laterally unconstrained	1124	403	420
LI-2200-IP5-SU	LI-2200	IP	Laterally unconstrained	1148	372	403
LI-2200-IP1-SC	LI-2200	IP	Laterally constrained	1034	406	440
LI-2200-IP2-SC	LI-2200	IP	Laterally constrained	1316	425	468
LI-2200-IP3-SC	LI-2200	IP	Laterally constrained	981	346	462
LI-2200-IP4-SC	LI-2200	IP	Laterally constrained	1133	415	413
LI-2200-IP6-SC	LI-2200	IP	Laterally constrained	1108	391	419
LI-2200-T1-SU	LI-2200	TTT	Laterally unconstrained	1015	464	264
LI-2200-T2-SU	LI-2200	TTT	Laterally unconstrained	893	354	249
LI-2200-T3-SU	LI-2200	TTT	Laterally unconstrained	1264	426	212
LI-2200-T4-SU	LI-2200	TTT	Laterally unconstrained	1061	381	205
LI-2200-T5-SU	LI-2200	TTT	Laterally unconstrained	862	490	213
LI-2200-T1-SC	LI-2200	TTT	Laterally constrained	1011	378	267
LI-2200-T2-SC	LI-2200	TTT	Laterally constrained	887	340	240
LI-2200-T3-SC	LI-2200	TTT	Laterally constrained	880	290	209
LI-2200-T4-SC	LI-2200	TTT	Laterally constrained	1026	368	213
LI-2200-T5-SC	LI-2200	TTT	Laterally constrained	887	334	215

IP-"In-Plane"; TTT-"Through-The-Thickness"

**Table D3. Summary of split Hopkinson pressure bar testing of FRCI-12.**

Test ID	Material	Orientation	Confinement	Strain rate at failure (1/s)	Strain rate average (1/s)	Peak stress (psi)
FRCI-12-IP1-SU	FRCI-12	IP	Laterally unconstrained	1773	464	320
FRCI-12-IP2-SU	FRCI-12	IP	Laterally unconstrained	823	393	341
FRCI-12-IP3-SU	FRCI-12	IP	Laterally unconstrained	781	290	346
FRCI-12-IP4-SU	FRCI-12	IP	Laterally unconstrained	860	306	352
FRCI-12-IP6-SU	FRCI-12	IP	Laterally unconstrained	752	259	353
FRCI-12-IP1-SC	FRCI-12	IP	Laterally constrained	751	300	326
FRCI-12-IP2-SC	FRCI-12	IP	Laterally constrained	810	322	343
FRCI-12-IP3-SC	FRCI-12	IP	Laterally constrained	860	294	339
FRCI-12-IP4-SC	FRCI-12	IP	Laterally constrained	899	317	345
FRCI-12-IP5-SC	FRCI-12	IP	Laterally constrained	902	343	337
FRCI-12-T1-SU	FRCI-12	TTT	Laterally unconstrained	1628	477	228
FRCI-12-T2-SU	FRCI-12	TTT	Laterally unconstrained	1375	444	218
FRCI-12-T3-SU	FRCI-12	TTT	Laterally unconstrained	1447	524	193
FRCI-12-T4-SU	FRCI-12	TTT	Laterally unconstrained	1604	493	191
FRCI-12-T5-SU	FRCI-12	TTT	Laterally unconstrained	1399	455	191
FRCI-12-T1-SC	FRCI-12	TTT	Laterally constrained	1295	431	215
FRCI-12-T2-SC	FRCI-12	TTT	Laterally constrained	1437	489	215
FRCI-12-T3-SC	FRCI-12	TTT	Laterally constrained	1609	531	183
FRCI-12-T4-SC	FRCI-12	TTT	Laterally constrained	1635	539	184
FRCI-12-T5-SC	FRCI-12	TTT	Laterally constrained	1420	493	188

IP-"In-Plane"; TTT-"Through-The-Thickness"

APPENDIX E

Effects of Strain Rates on the Strength and the Young's Modulus of the TPS Materials

Uniaxial Compression / SHPB

Legend:
- LI-900 IP (○)
- LI-900 TTT (●)
- LI-2200 IP (□)
- LI-2200 TTT (■)
- FRCI-12 IP (△)
- FRCI-12 TTT (▲)
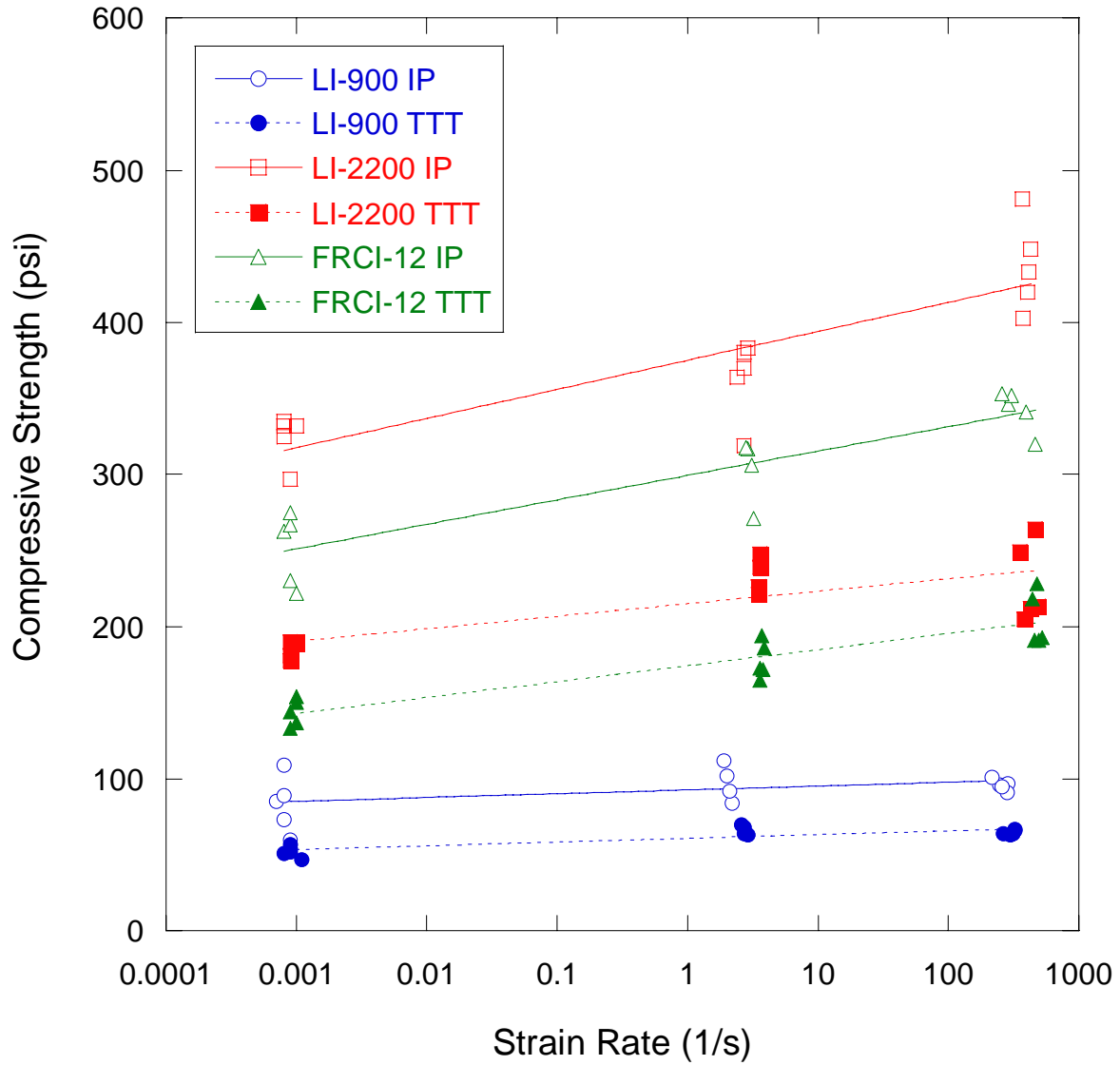
Regression equations:
- y = 92.849 + 2.4916log(x)   R= 0.436
- y = 60.896 + 2.4371log(x)   R= 0.83173
- y = 375.07 + 19.078log(x)   R= 0.86236
- y = 215 + 8.2021log(x)   R= 0.7392
- y = 299.45 + 16.058log(x)   R= 0.8995
- y = 174.46 + 10.523log(x)   R= 0.90089

Figure E1. Effects of strain rates on the strength of the TPS materials under compression (x: strain rate and y: compressive strength in regression equations).
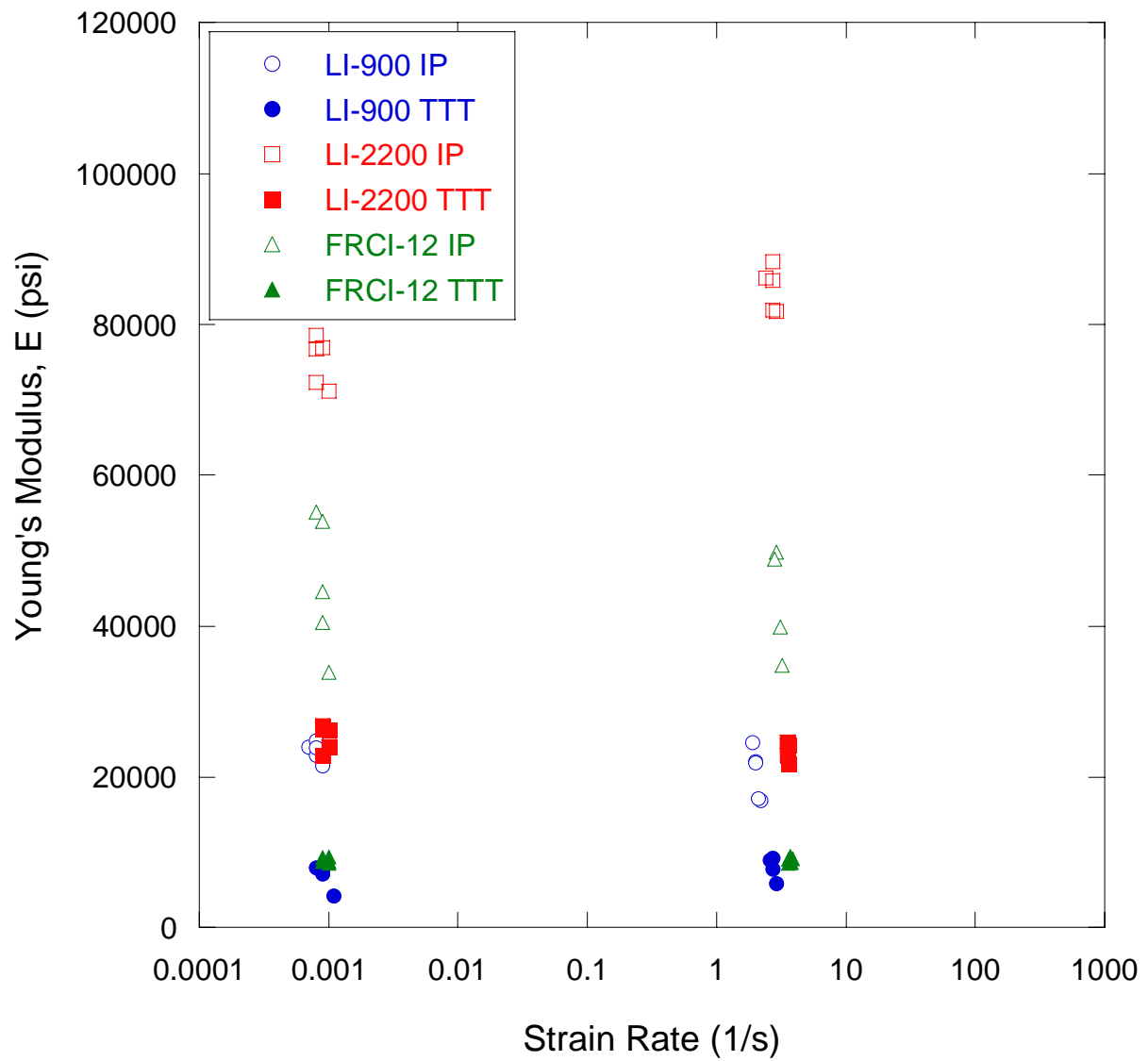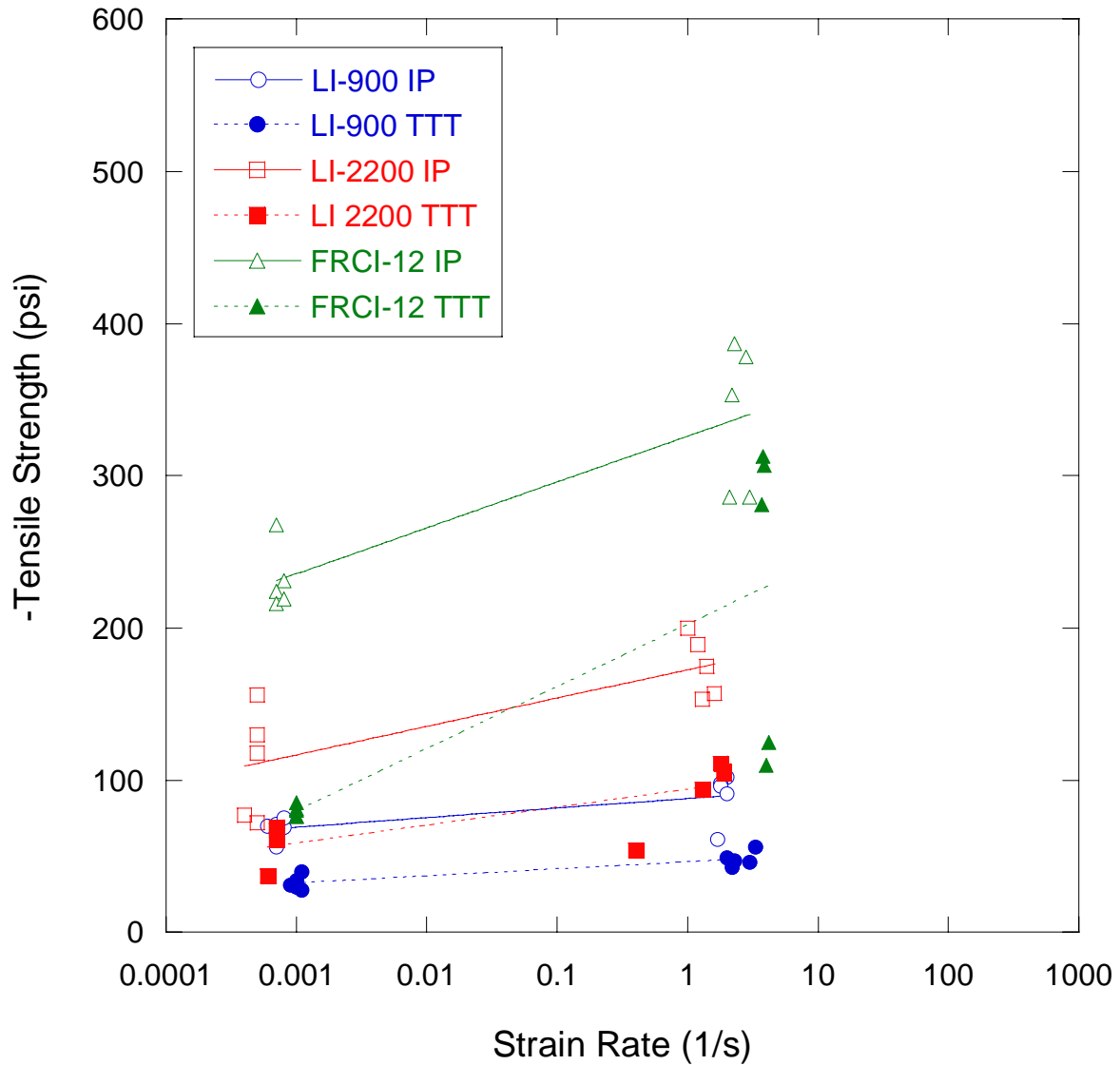
Uniaxial Compression / SHPB

Figure E2. Effects of strain rates on the Young's modulus of the TPS materials under compression.

Uniaxial Tension Test

y = 87.994 + 6.3227log(x)   R= 0.6915
y = 46.406 + 4.6337log(x)   R= 0.88476
y = 172.64 + 18.645log(x)   R= 0.77471
y = 94.218 + 11.841log(x)   R= 0.77816
y = 326.11 + 30.139log(x)   R= 0.84238
y = 202.59 + 40.869log(x)   R= 0.75199

Figure E3. Effects of strain rates on the tensile strength of the TPS materials (x: strain rate and y: - tensile strength in regression equations).
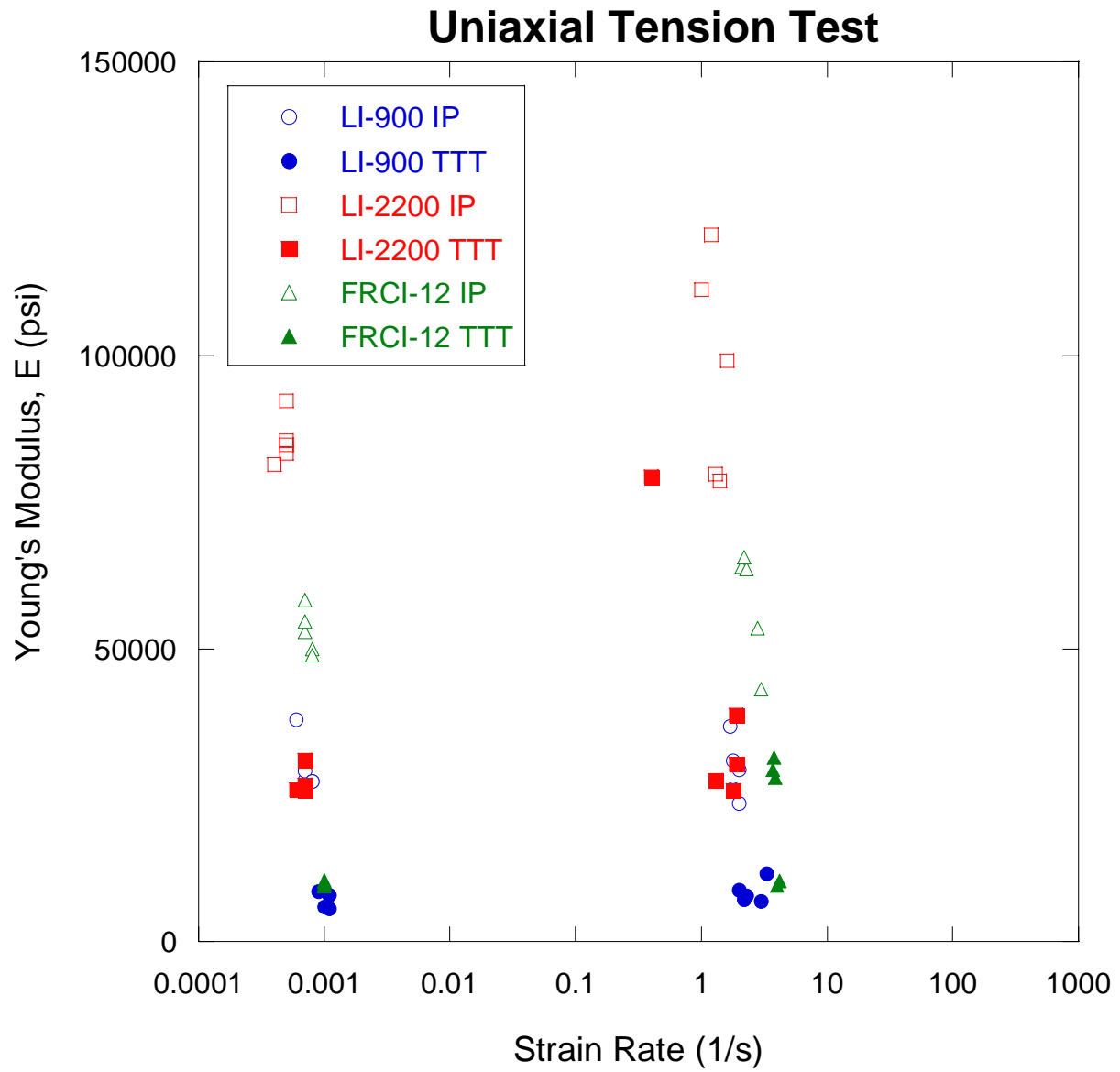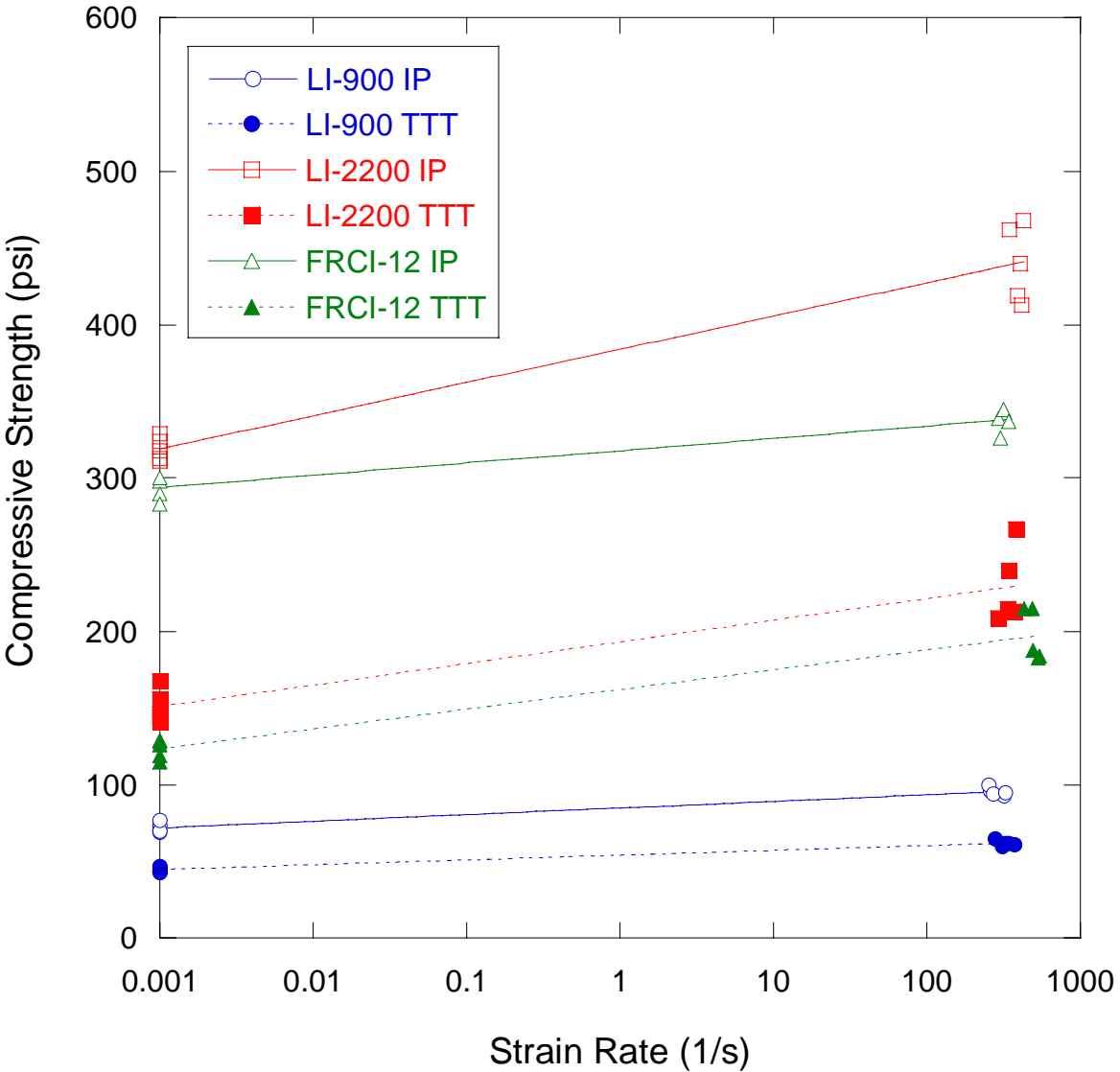
Figure E4. Effects of strain rates on the Young's modulus of the TPS materials in tension.

Uniaxial Strain / SHPB

Legend:
- LI-900 IP (blue open circle)
- LI-900 TTT (blue filled circle)
- LI-2200 IP (red open square)
- LI-2200 TTT (red filled square)
- FRCI-12 IP (green open triangle)
- FRCI-12 TTT (green filled triangle)

y = 84.892 + 4.359log(x)   R= 0.97436
y = 54.162 + 3.1179log(x)   R= 0.98273
y = 384.07 + 21.677log(x)   R= 0.96519
y = 193.2 + 14.097log(x)   R= 0.91818
y = 317.92 + 8.0424log(x)   R= 0.95954
y = 162.17 + 12.898log(x)   R= 0.95511

Figure E5. Effects of strain rates on the compression strength of the TPS materials under a confined (or uniaxial strain) condition (x: strain rate and y: compressive strength in regression equations).
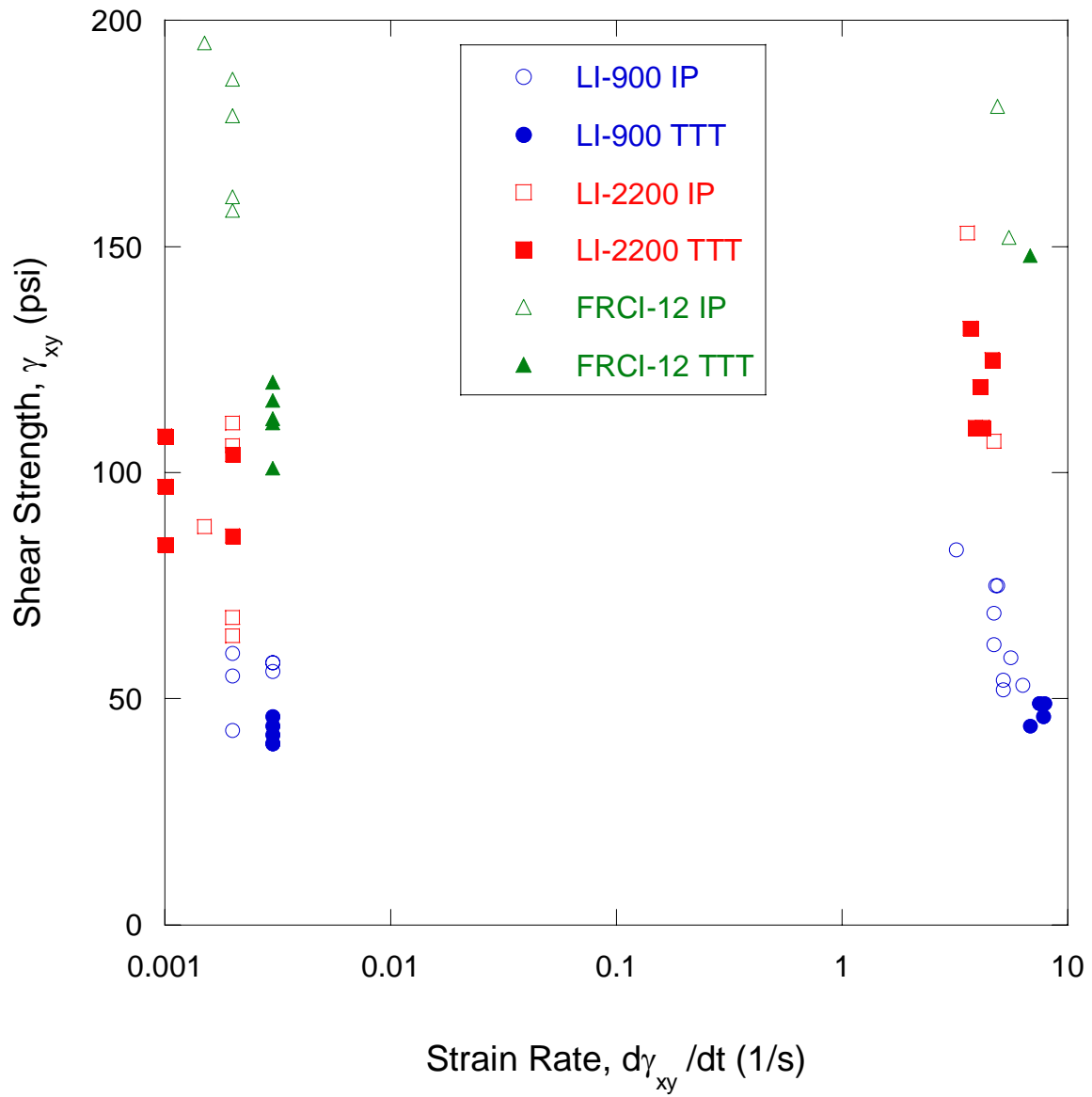
Shear Test

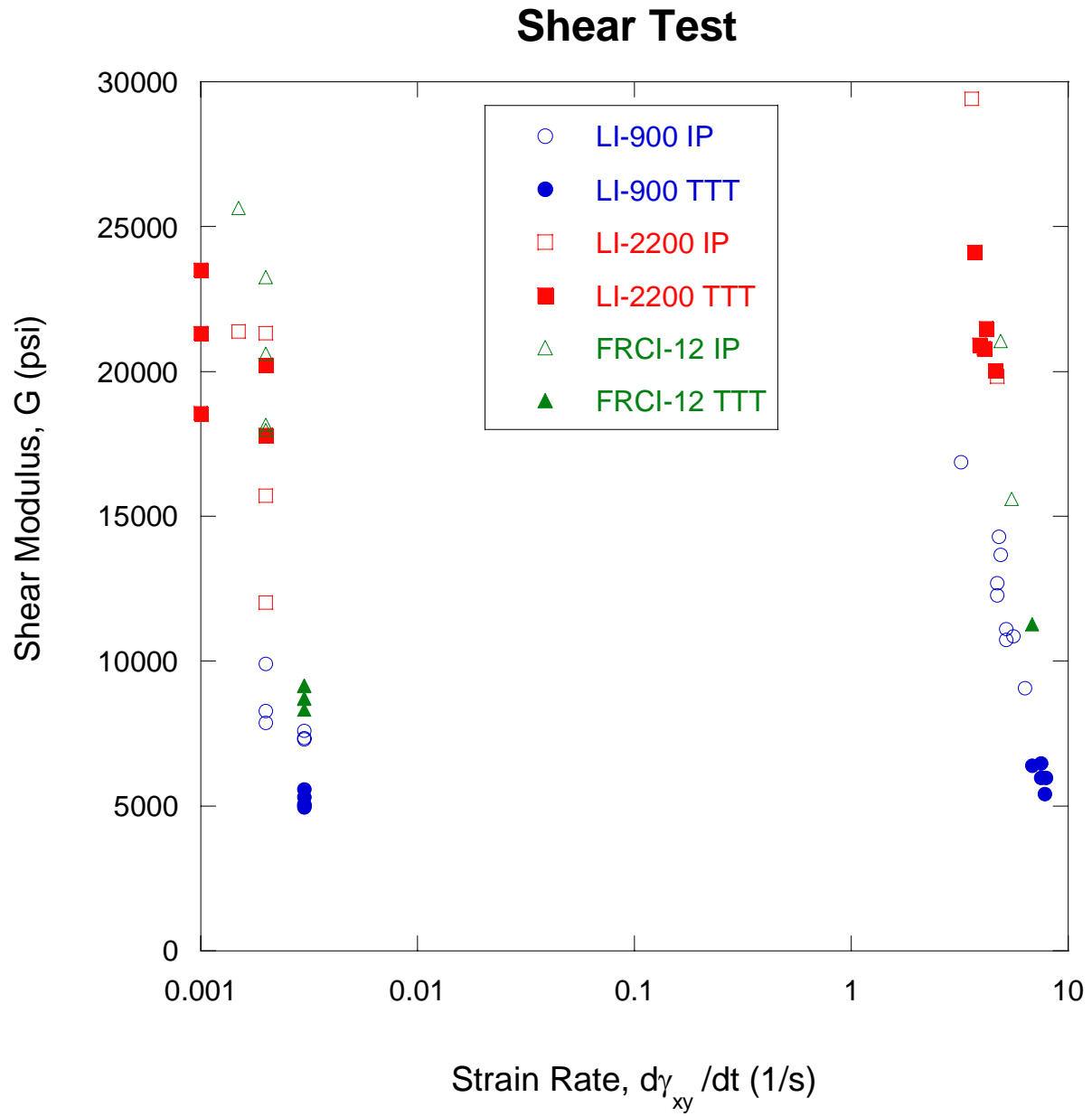**Figure E6. Effects of strain rates on the shear strength of the TPS materials.**

Figure E7. Effects of strain rates on the shear modulus of the TPS materials.

DISTRIBUTION

Sandia National Laboratories
P.O. Box 5800
Albuquerque, NM 87185

1	MS 0372	K. W. Gwinn, 9126
1	MS 0701	P. J. Davies, 6100
1	MS 0751	L. S. Costin
1	MS 0701	J. A. Merson, 6110
5	MS 0751	M. Y. Lee, 6117
1	MS 0751	T. W. Pfeifle, 6117
1	MS 1031	R. D. Hardy, 6117
1	MS 1031	D. R. Bronowski, 6117
1	MS 1031	J. H. Hofer, 6117
1	MS 0731	823/Library, 6850
2	MS 0899	Technical Library, 9616
1	MS 9018	Central Tech. Files, 8945-1

NASA Johnson Space Center
Mail Code ES3
Building 13, Room 131
2101 NASA Parkway
Houston, Texas 77058
john.kowal@jsc.nasa.gov
John Kowal

The Boeing Company
13100 Space Center Blvd
MC HB6-30
Houston, TX 77059-3556

Paul Parker
Jeremy Brand
Paul Parker   paul.a.parker@boeing.com
Jeremy Brand   jeremy.h.brand@boeing.com

PO Box 21233 MC721Z-K085
Kennedy Space Center, Fl 32815-0233

Dan Bell   dan.r.bell@boeing.com

5301 Bolsa Ave. MC H021-F120
Huntington Beach, CA 92647-2099

Joel Slenk   joel.e.slenk@boeing.com